

Article

Transport of Sediment Mixtures in Steady Flow with an Extra Contribution of Their Finest Fractions: Laboratory Tests and Modeling

Jerzy Zawisza ^{1,*}, Iwona Radosz ¹ , Jarosław Biegowski ² and Leszek M. Kaczmarek ¹ 

¹ Faculty of Civil Engineering, Environmental and Geodetic Sciences, Koszalin University of Technology, 75-453 Koszalin, Poland

² Institute of Hydro-Engineering, Polish Academy of Sciences, 80-328 Gdańsk, Poland

* Correspondence: jerzy.zawisza@tu.koszalin.pl

Abstract: This paper presents the results of experimental studies on the transport of water-sandy mixtures with the content of very fine non-cohesive fractions in steady flow. The flow and shear velocity measurements as well as the measurements of sediment amount in the trap and control area were conducted. A theoretical model of the vertical structure of both velocity and concentration of sediment non-cohesive fractions as well as vertical mixing and sorting is presented here for transport calculations. The interaction effects between fractions are included, especially the influence of fine fractions in the mixture on transport of coarser fractions. The model provides an agreement between measurements and calculations of transport rate and grain size distributions of poorly sorted mixtures within plus/minus a coefficient of two. Further, the present model is used for calculating the limited contribution of very fine fractions in sediment due to deficit of those fractions in the bed. Again, the compliance of the calculations of sediment transport according to measurements is achieved. The satisfactory agreement between the calculations of grain size distributions and measurements is also found.

Keywords: steady flow; sediment transport; sediment mixture; grain size distribution; fine non-cohesive fraction



Citation: Zawisza, J.; Radosz, I.; Biegowski, J.; Kaczmarek, L.M. Transport of Sediment Mixtures in Steady Flow with an Extra Contribution of Their Finest Fractions: Laboratory Tests and Modeling. *Water* **2023**, *15*, 832. <https://doi.org/10.3390/w15050832>

Academic Editor: Carl L Amos

Received: 7 December 2022

Revised: 14 February 2023

Accepted: 15 February 2023

Published: 21 February 2023



Copyright: © 2023 by the authors. Licensee MDPI, Basel, Switzerland. This article is an open access article distributed under the terms and conditions of the Creative Commons Attribution (CC BY) license (<https://creativecommons.org/licenses/by/4.0/>).

1. Introduction

The dynamics of sediments containing fine and coarse non-cohesive particles is the result of their transport, which is accompanied by mass and momentum exchange processes, leading to the formation of high-concentration suspensions and their settling in the bed substrate. There are numerous studies related to the dynamics of sediments transported and sorted in coastal regions and rivers, starting from [1] to [2–5] and [6,7] up to [8–12], which include both theoretical and experimental research. Works related to the transport of sediments were conducted in several directions. The first one is the use of formulas of Meyer-Peter and Müller (abbreviated to “MPM”) [13], because formulas of this type, due to the speed of calculations are used in large software packages. The second direction of research was the development of models of homogeneous sediment transport, taking into account the interactions between sediment and water. Another direction of research is the development of models for transport of granulometrically heterogeneous sediments [14–16], taking into account the interactions between different fractions of sediment mixture. Many of the works [17–19] represent a probabilistic approach to bedload transport, in which the motion of particles is modeled on the basis of probability density functions for velocities and grain accelerations. Recently, the Lagrangian modelling of sediment transport has also been widely used e.g., [20]. Lagrangian modeling, although very precise and capable of determining exact paths of separate particles, is less effective when large data sets are considered. Hence, double averaging methodology (DAM, Double-Averaging Methodology)

methods are employed e.g., [21–23]. However, an important issue is the use of suitable dense suspensions, i.e., for collision-dominated and contact-dominated particle transport [22]. This is particularly important because there is an upper limit for the saltation regime, above which collision suspension takes place [24–26].

Thus, although significant progress has been made, many questions of fundamental importance still await answers. In particular, the role of fine and very fine fractions in transport of sediment mixture, and the influence of those fractions on transport of coarse fractions is still an open question. Since the issue of sediment transport is strongly related to the generation and migration of bottom forms such as ripples and bars, these phenomena are part of the problem and should also be included in the calculations. The issues of sediment transport above the seabed with and without bed forms were taken up by [27–29], and recently by [30–32] for rivers and [33–36] for wave-current conditions. The extensive studies on hydrodynamics [37] as well as on morphological characteristics due to sand transport were conducted by [38–40] and recently by [41,42]. However, those works do not explain the whole erosion process, resulting from the presence in the substrate of very fine sandy fractions, especially the limited contributions of very fine non-cohesive fractions in sediment transport due to deficit of those fractions in the bed. The transport of very fine fractions increases exponentially as the diameter of the grains decreases. Therefore, there may be a situation in which the availability of these fractions in the active layer of the seabed will be limited. Meanwhile, in the modelling of sediment transport, is commonly assumed that each fraction is available without limitations.

It should be expected that the presence of fine non-cohesive fractions in the sediment causes decrease in the critical shear stress at incipient motion of sediments and, on the other hand, an increase in the velocity of the sediments at the boundary between bedload and contact layer. It results in an increase in the amount of the transported sediments. In the saltation layer above the bottom, the distances between the grains of sand increase and the release of grains of fine fractions occurs. Thus, through the velocity at the lower limit of the contact layer, i.e., at top of the grain-collision sublayer, the influence of fine and very fine fractions is revealed. As a result of the interactions, the fine fractions in the bedload layer are slowed down by the coarser ones, while the latter are accelerated. In other words, coarser sediments in the mixture are more exposed to the flow, whereas thinner sediments are hiding among the coarser ones. The hiding and exposure effects can affect the transport rates of sediment grain fractions. Ref. [43] measured a wide range for five different sand/gravel mixtures in laboratory flume. They showed as sand content increased, gravel transport rates increased by orders of magnitude, even though the proportion of gravel in the bed decreased. In turn, as a result of vertical sorting, the smallest fractions are raised high above the bottom significantly increasing both in the concentration and transport of suspended sediments in this area. As recent works on sediment transport in the wave motion have shown [44,45], the increased concentration of suspended fine fractions causes a significant increase in the transport of coarse fractions. On the other hand, it means a deficit of fine fractions in the bottom, resulting in limited availability of these fractions. This deficit of the finest fractions in the active layer of the bottom may in turn cause a reduction in the transport of these fractions.

The starting point for modeling the influence of very fine non-cohesive fractions on the transport of sandy sediments, is the transport model for uniform and heterogeneous sediment transport proposed for wave motion by [46,47]. The initial assumption of this model is the requirement that the mechanism causing sediments to be picked up from the bottom and setting them in motion is shear stresses acting on the bottom. Thus, the “reaction” of the bottom to hydrodynamic conditions occurs. In the hydrodynamic equilibrium [48,49], the stream of sediments taken out from the control area of the bottom is equal to the stream of sediments falling onto the bottom in the adjacent control area. It means that the entire sediment, transported both in the bedload and suspended layers, comes exclusively from the bottom of the control area under consideration. It was postulated that due to the different nature of physical processes occurring at different distances from the

bottom, it is necessary to use different assumptions and equations to describe the vertical structure of sediment transport. The proposed multilayer model for uniform sediment transport in rivers [50] and for non-uniform sediment transport in the wave motion [51,52] further developed in the works [44,45], presents three main layers with separate sublayers.

The scope of this work was the study of the intensity of transport of a mixture of sandy sediments, containing a significant amount of fine and very fine non-cohesive fractions. The study was dedicated to investigating the effect of those fractions on the transport of the coarse fractions in the mixture and on the transport of the whole mixture.

The experimental results were compared with the results of a theoretical analysis based on the proposed three-layer model of heterogeneous sediment transport. The influence of the finest fractions in the mixture on transport of the coarser fractions is included in the modeling. In addition, the present model is used for calculating the limited contribution of very fine fractions in sediment transport due to available deficit of those fractions in the seabed.

2. Materials and Methods

2.1. Experiment Gdańsk, 2021

The experiments were conducted in a recirculating flow channel adapted to the specifics of the sediment transport study. Research station located in the laboratory at the Institute of Hydro- Engineering of the Polish Academy of Sciences (IBW PAN) in Gdańsk. A diagram of the test bench is shown in Figure 1.

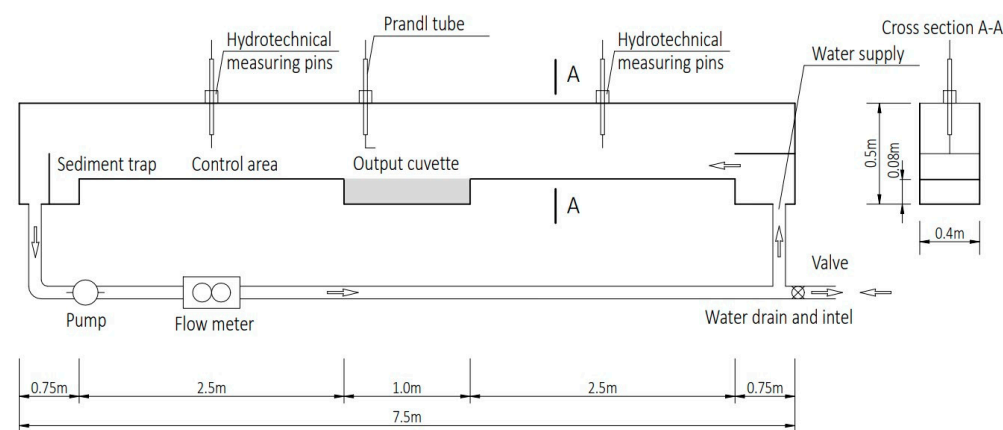


Figure 1. Experimental setup for steady flow measurements Gdańsk 2021.

The main purpose of the measurements was to collect experimental data documenting the magnitude of sediment transport and the magnitude of erosion inside the output cuvette. The velocity of sediment flow from the output cuvette to the control area, the amount of sediment retained in the control area and in the trap were measured. Measurements of bathymetric changes in the calculation area were made. In addition, analyses of granulometric compositions of sediment samples taken before experiments and of sediment samples taken from the trap and control area after the completion of each measurement series, were performed.

The Gdańsk 2021 experiments were conducted on a test stand, the main element of which was an open channel with a length of 7.5 m and a cross-section of 0.4×0.5 m. The channel, exit cuvette and sediment traps in the bottom of the channel, are made of the waterproof plywood 0.02 m thick. The roughness of the channel bottom was achieved by gluing sand with a diameter of $0.20 \text{ mm} \leq d \leq 0.25 \text{ mm}$ to the surface. The inclination of the channel bed was constant and amounted to 0.002 (2‰). The channel can be divided into several sections:

- a 0.73 m long outflow section, with a bottom inlet supplying the channel with water;
- starting section with a length with a length of 2.5 m;

- a cuvette with the input sediment, i.e., a depression along the entire channel, 1 m long and 0.08 m high;
- the test section 2.5 m long;
- sediment trap, in the form of another cuvette, i.e., a depression channel 0.73 m long and 0.08 m high, with a bottom inlet and outlet.

The channel was integrated with a pump (Grundfos: 50 Hz, $Q = 38$ L/s) with a system of hoses of 0.075 m in diameter working in a closed system, a set to control and measure (Danfoss), and a set of two Siemens flowmeters with accuracy of 0.25%. The stand was equipped with a Prandl tube and two hydraulic pins. The tests were conducted according to the following procedure:

1. Filling the cuvette with the water-saturated sediment. Placing the wet sediment in the cuvette prevented formation of air bubbles in the deposited mixture;
2. Taking a sample from the container filled with sediment prepared for testing;
3. Leveling the sediment to the edge of the cuvette and removing the remains of sediment from the vicinity of the cuvette;
4. Filling the channel up to the water depth $H = 0.05$ m;
5. Performing a test for a given flow (Times for individual tests are given in Table 1);
6. Measurements of the velocity over the bottom using the Prandtl tube (0.1 m above the lower edge of the cuvette, in the period between the flow stabilization and the development of wrinkles);
7. Water removal from the channel after the test is completed;
8. Collection of sediment from the trap and control area;
9. Measurement of sediment volume captured in the sand trap;
10. Documentation of bathymetry in a cuvette by taking photos, performing a bathymetric measurement;
11. Collecting sediment samples for sieve analysis;
12. Removal of sediment from cuvette and its cleaning.

The basic parameters of experiments in the flow channel of IBW PAN where Gdańsk 2021 experiment was conducted, the granulometric characteristics of the input sand and the sediments taken from the trap and the control area are shown in Table 1. As can be seen from the prepared grain size curve (Figure 2), the analyzed sediment is sand with a very large number of fine fractions ($d_i < 0.22$ mm) and with median diameter of $d_{50} = 0.22$ mm.

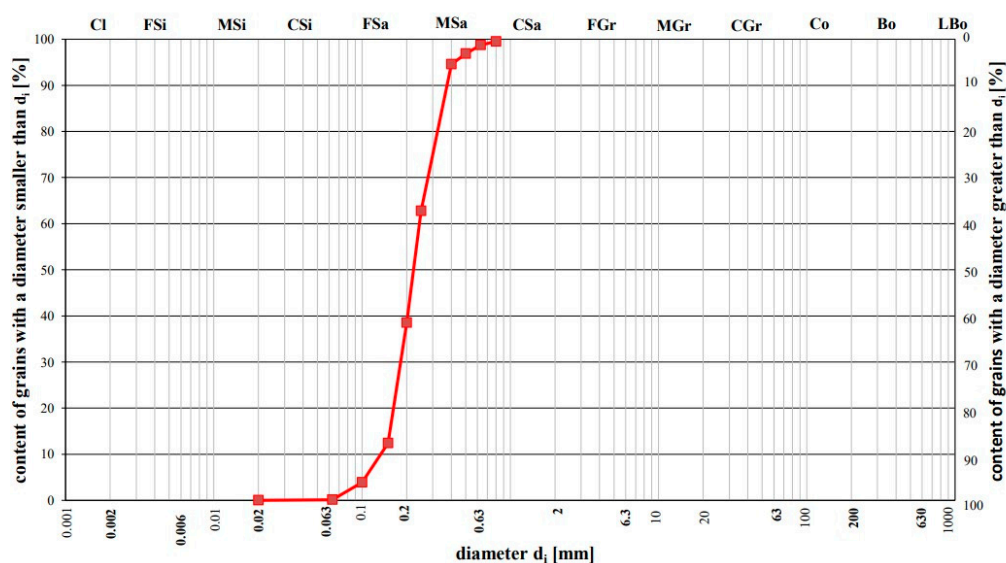


Figure 2. Grain size distribution of input quartz sand used in the Gdańsk 2021 experiment.

Table 1. Main parameters and transport results of the Gdańsk 2021 experiment.

TR Test	Flow Rate [L/s]	\bar{u} -Depth Averaged [m/s]	Friction		Rep. of Tests [-]	Test Time [s]	Sediment Transport Maximum Mean Minimum [m ³ /ms]	Fractions d ₉₀ /d ₅₀ /d ₁₀ [mm]	$Re = \frac{uH}{\nu}$ [-]
			u_{f*} [m/s]	θ^* [-]					
Input sand								0.23/0.22/0.14	
TR_0_7	7.0	0.5000	0.0097	0.2587	2	3600	8.00·10 ⁻⁹ 5.50·10⁻⁹ 3.00·10 ⁻⁹	0.23/0.14/0.03	13,462
TR_0_8	8.0	0.5715	0.0158	0.0690	4	3600	1.90·10 ⁻⁸ 6.60·10⁻⁷ 3.43·10 ⁻⁶	0.23/0.21/0.11	15,385
TR_0_9	9.0	0.6429	0.0177	0.0862	3	3600	7.59·10 ⁻⁷ 6.84·10⁻⁷ 5.61·10 ⁻⁷	0.24/0.21/0.12	17,308
TR_0_10	10.0	0.7143	0.0185	0.0949	3	3600	7.95·10 ⁻⁷ 7.38·10⁻⁷ 6.80·10 ⁻⁷	0.24/0.21/0.11	19,231
TR_0_11	11.0	0.7857	0.0194	0.1035	3	3600	1.16·10 ⁻⁶ 1.08·10⁻⁶ 1.00·10 ⁻⁶	0.24/0.22/0.12	21,154
TR_0_12	12.0	0.8571	0.0201	0.1121	3	3600	1.52·10 ⁻⁶ 1.29·10⁻⁶ 1.06·10 ⁻⁶	0.26/0.24/0.13	23,077
TR_0_13	13.0	0.9285	0.0244	0.1638	3	1800	6.77·10 ⁻⁶ 4.86·10⁻⁶ 2.94·10 ⁻⁶	0.24/0.22/0.12	25,000
TR_0_14	14.0	1.0000	0.0273	0.2070	3	900	1.33·10 ⁻⁵ 9.60·10⁻⁶ 5.91·10 ⁻⁶	0.26/0.24/0.14	26,923
TR_0_15	15.0	1.0714	0.0306	0.2587	3	900	1.80·10 ⁻⁵ 1.44·10⁻⁵ 1.07·10 ⁻⁵	0.25/0.22/0.11	28,846

It is worth noting that the median diameter d_{50} of sediments retained in the trap and control area differs from the values measured for the input sand. In the regime of more intensive transport, this value is larger than in the input. The above result is not intuitive, because very fine fractions are more mobile than coarse grains. Therefore, their greater contribution to the transport should be expected. The reason for this should be sought in the limited volume of these fractions in the layer of sediments filling the cuvette.

For water level measurements and bathymetry tests, a set of hydrometric pins were used, enabling readings with an accuracy of 0.1 mm. Laboratory tests were conducted in the wide range of flow rates, from 2 to 15 L/s. The measured vertical velocity distribution was approximated by a logarithmic profile from which the friction velocity was determined.

In the Figure 3 both the results of all measurements of sediment transport rate obtained during Gdańsk 2021 experiments as well as the mean values of the measurement series

within ‘TR tests’ (see Table 1) are presented in terms dimensionless transport functions of Φ defined as:

$$\Phi = \frac{q}{(s - 1)gd_r^3} \tag{1}$$

where $q[m^2/s]$ is the sediment transport rate; $d = d_r$ is the representative diameter for sediment mixture in the dense layer, assumed as $d_r = d_{50}$; $s = \rho_s/\rho$ is the relative density; ρ_s is the density of sediments; g is the acceleration due to gravity and ρ is water density, while non-dimensional shear stress θ'_* is defined as:

$$\theta'_* = \frac{u'_{f*}{}^2}{(s - 1)gd_r'} \tag{2}$$

where u'_{f*} is the shear velocity.

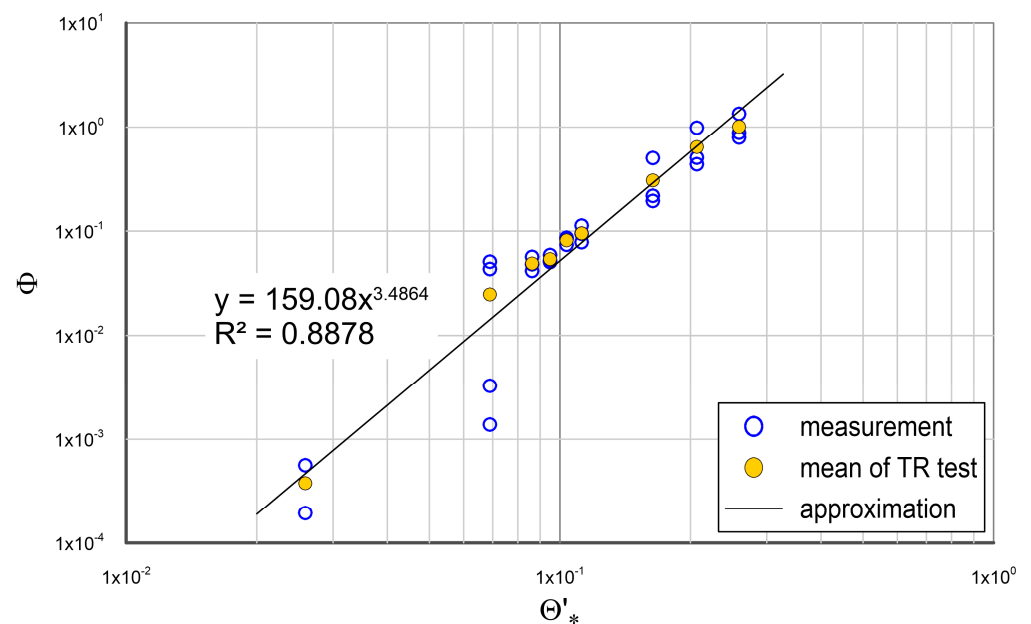


Figure 3. The approximation of transport measurements (Gdańsk 2021 experiments) and the mean values of measurement tests by curve with a coefficient of determination $R^2 = 0.8878$.

The collected samples were subject to granulometric analysis in the geotechnical laboratory of the Koszalin University of Technology. For this purpose, a Micro LAB sieve shaker (model: LPzE-2e) was used. Measurements were made using the “dry” method for all sediment samples. The samples were dried at $100 \pm 0 \text{ }^\circ\text{C}$ for 24 h before granulometric analysis. Examples of measured grain size distributions for flows of 8 L/s and 14 L/s are shown in Figure 4.

The sample results shown in the Figure 4 confirm the observations on the limited availability of very fine fractions in the bottom. In particular, in the range of more intense flows (Figure 4b) with increasing transport rates the share of coarse fractions in the retained sediment increases, while the contribution of finer fractions decreases as a result of their deficit in the bottom.

It is assumed in the model that velocity u profile reaches a logarithmic profile at certain distance from the bottom with the origin $z = \frac{k_s}{30}$ at the bottom:

$$u = \frac{u'_{f*}}{\kappa} \ln \frac{z}{\frac{k_s}{30}} \tag{3}$$

were k_s is the skin roughness assumed as $k_s = 2.5d_{50}$ and κ is von Karman constant, which is assumed as 0.40. The vertical axis z is directed upward.

In order to determine the friction velocity u'_{f*} from the experiments it is proposed to find the friction velocity value from Equation (3) for each measured velocity $u(z)$ at the level z . Then the findings the friction velocity are averaged over the depth. Finally, the depth average value $\overline{u'_{f*}}$ was assumed as friction velocity taken the measurements.

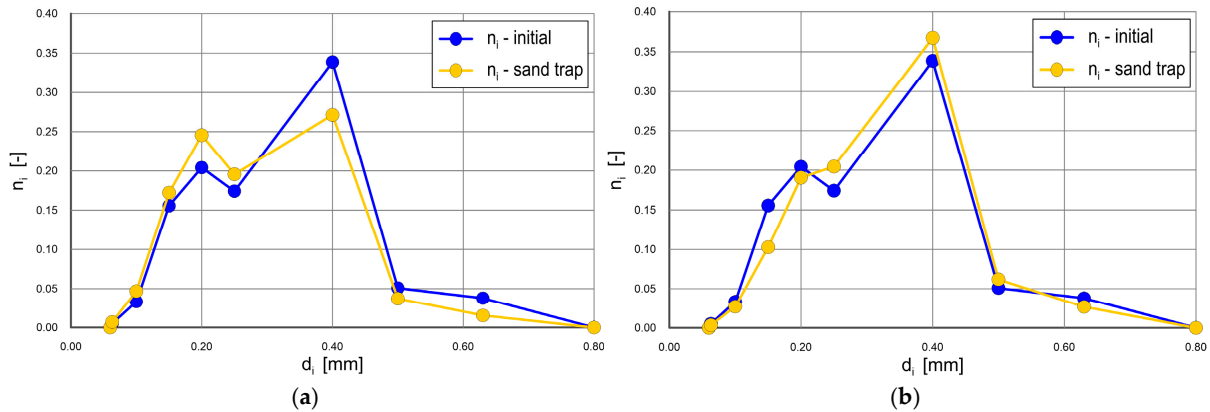


Figure 4. Grain size distribution of quartz sand in the trap at the flow (a) 8 L/s and (b) 14 L/s in the Gdańsk 2021 experiment.

Figure 5a shows exemplary results of the measured vertical velocity profile $u(z)$ in comparison with logarithmic profile characterized by the depth average shear velocity $\overline{u'_{f*}}$. Figure 5b shows the shear velocities u'_{f*} taken from $u(z)$ measurements in comparison with the depth average value $\overline{u'_{f*}}$.

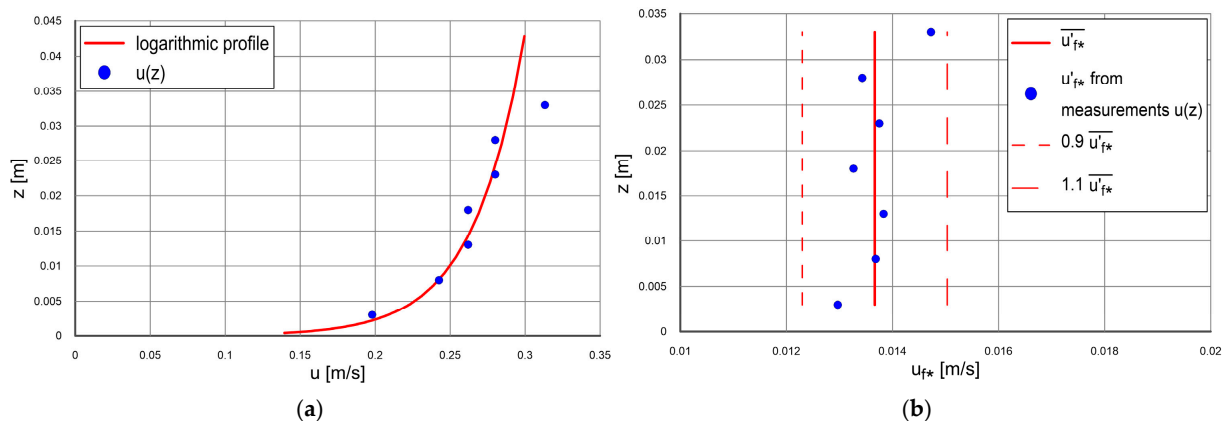


Figure 5. Exemplary vertical profile: (a) vertical velocity profile for the measured $u(z)$ and the logarithmic profile with the depth average shear velocity $\overline{u'_{f*}}$; (b) the shear velocities taken from $u(z)$ measurements in comparison with the dept average value $\overline{u'_{f*}}$.

As it is seen from Figure 5b the values of friction velocities taken from $u(z)$ measurements are in the range $0.9\overline{u'_{f*}} \div 1.1\overline{u'_{f*}}$.

2.2. Experiment by Elhakeem and Imran (2012) [53]

Elhakeem and Imran in 2012 [53] presented experiments conducted in the laboratory of the University of South Carolina. These tests were conducted in a tilting channel with a length of 10 m, width of 0.20 m and a depth of 0.4 m. The test stand was equipped with a closed water supply system. In addition, it was equipped with a flap, mobile trolleys, a

feeder and sediment collector, a sediment sampler and instruments for measuring discharge, water depth, substrate geometry and speed in the loading layer (Figure 6).

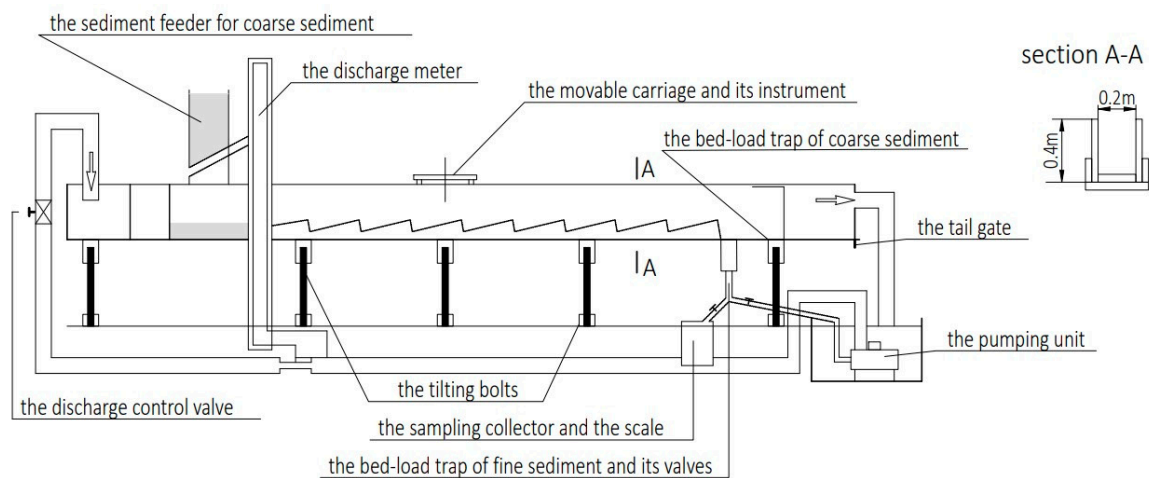
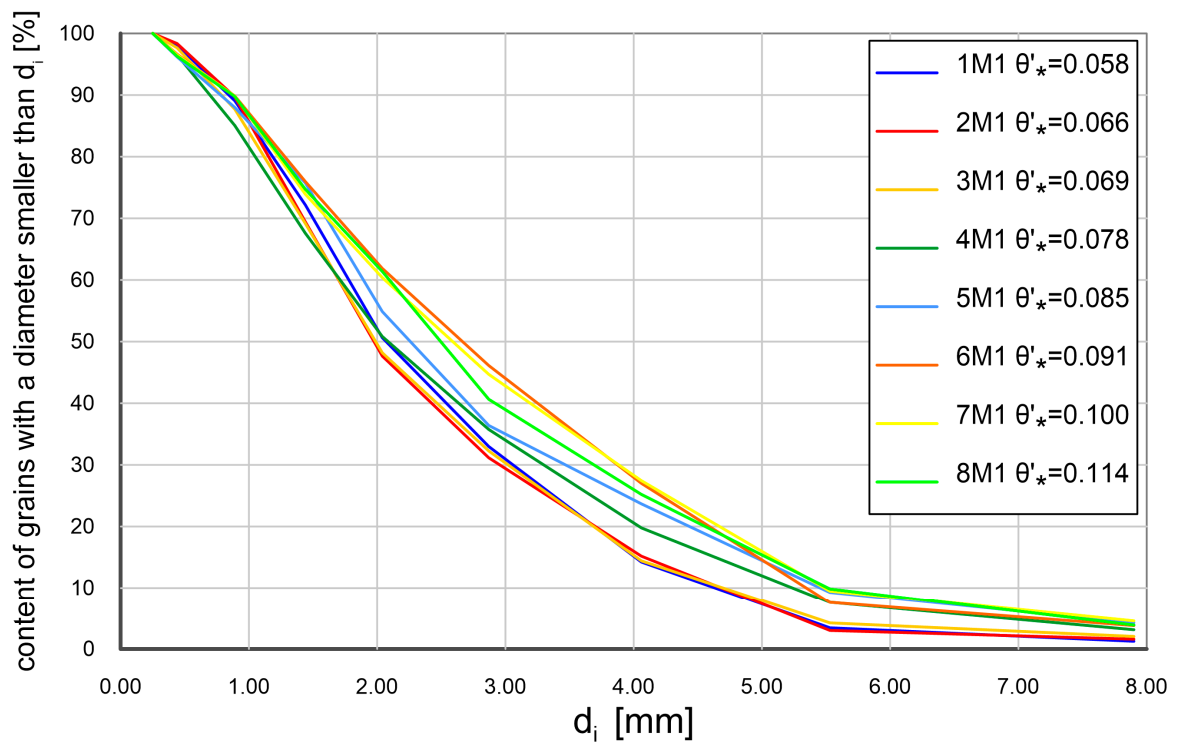


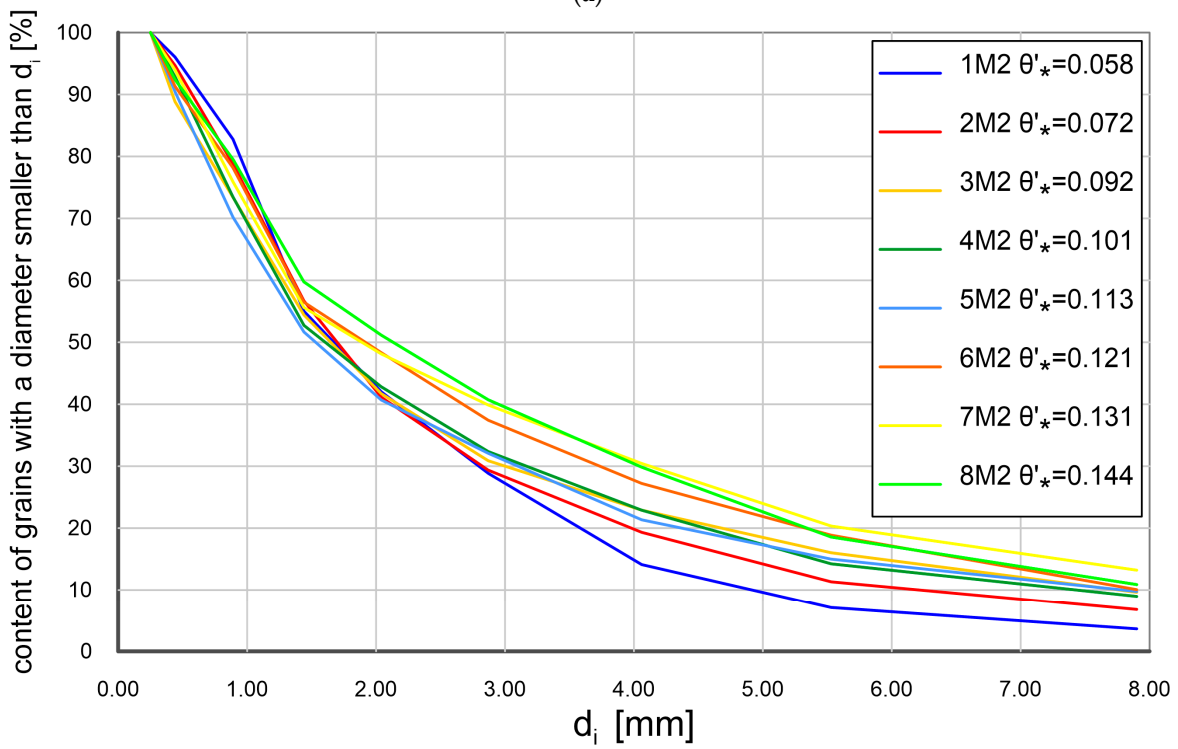
Figure 6. Experimental setup for steady flow measurements by Elhakeem and Imran (2012) [53].

The laboratory tests presented in [53] were conducted in similar hydrodynamic conditions as the Gdańsk 2021 experiments. The tests [53] were conducted for natural sands and gravels with a specific gravity of 2.65 g/cm^3 . The experiments were conducted for flows ranging from 9 to 15 L/s at the average velocities from 0.429 to 9.676 m/s. The duration of the tests ranged from 1800 to 3600 s. The inclination of channel was from 0.0037 to 0.0062, and the water depths were from 0.096 to 0.134 m. A total of 32 runs were conducted under the equilibrium condition within the lower regime, primarily dunes. During the run, coarse material ($d_i > 2.87 \text{ mm}$) was trapped at the downstream end of the flume (Figure 6), collected manually from the coarse sediment trap, and fed into the sediment feeder at the upstream section of the flume.

Four mixtures of M1–M4 from almost homogeneous sands to poorly sorted mixtures of sand and gravel were used for testing. The initial samples of sediments used in the experiments as well as the samples of the sediments collected in traps were subjected to granulometric analysis. In Figure 7 the initial grain size distributions for different mixtures from M1 to M4 in tests 1 to 8 by Elhakeem and Imran [53] are shown. The tests 1 were conducted for the smallest Shields stress θ'_* of the geometric mean size of the sediment mixture (with d_r in Equation (2) equal to geometric mean size), while the tests 8 were conducted for the biggest Shields stress (see Figure 7). It can be observed (Table 2) that as the measured rate of transport q [g/m/s] increases the measured content of coarse fractions and median d_{50} also increases. In this case, the reason for this should be expected in the interactions of fine and coarse fractions, causing an increase in the share of the latter in transport of the whole mixture. This effect appears to be similar to that of the experiments performed by Wilcock et al. [43]. They showed as sand content increased, gravel transport rates increased by orders of magnitude, even though the proportion of gravel in the bed decreased. As a result of the interaction between the sediment fractions, the fine fractions in the mixture are slowed down by the coarse fractions, while the latter are accelerated.



(a)



(b)

Figure 7. Cont.

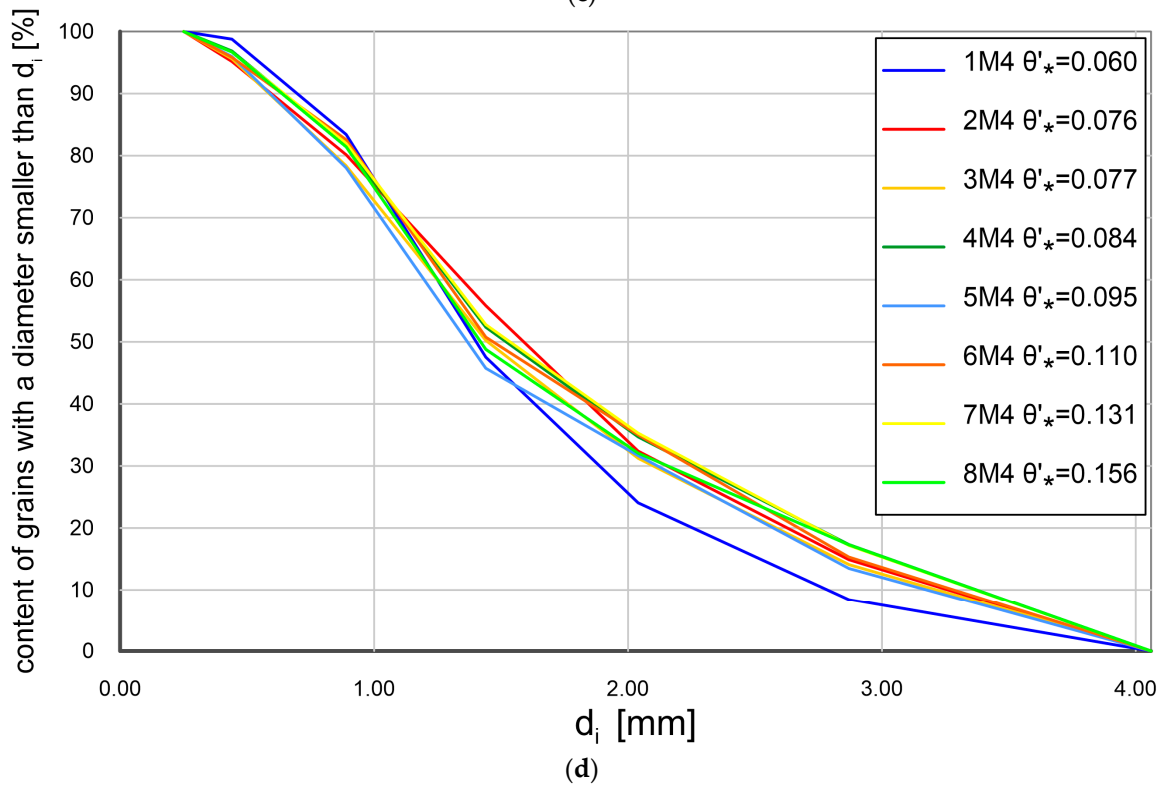
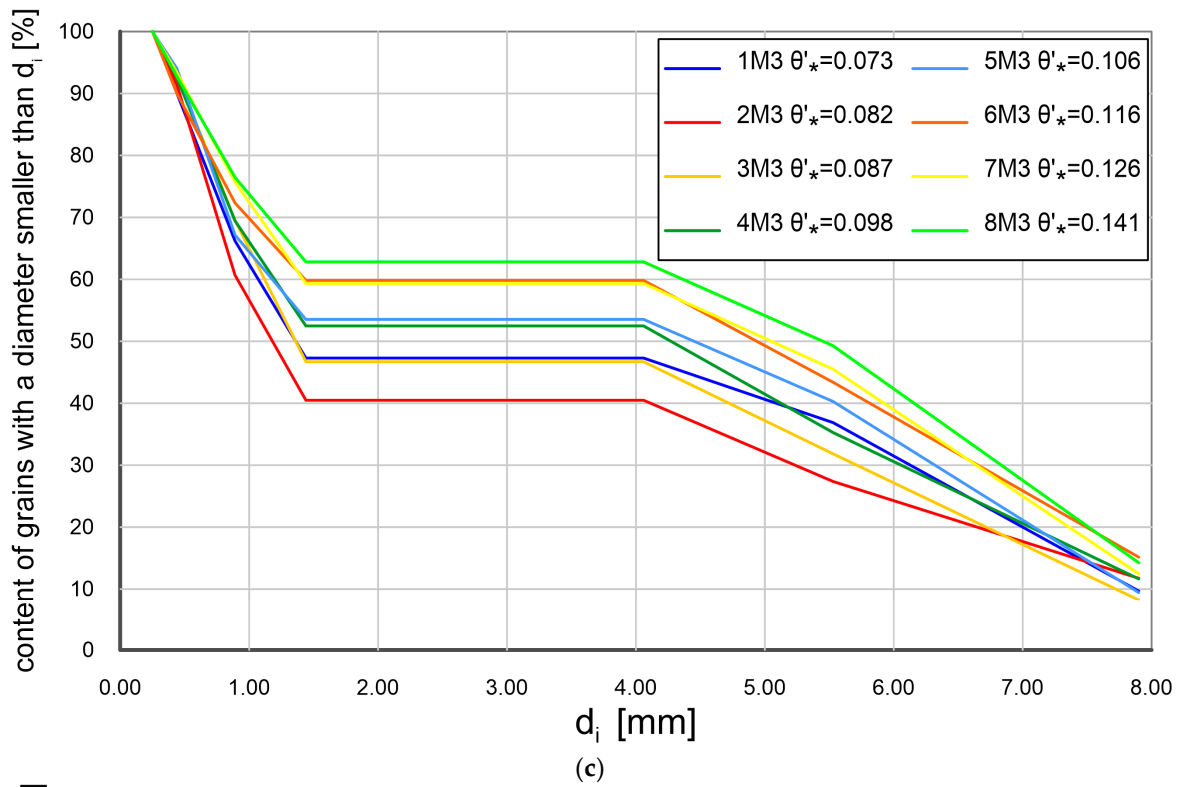


Figure 7. Particle size distribution determined for various mixtures caught in a trap in the experiments by [53], tests 1–8 for the initial particle size distribution (a) M1, (b) M2, (c) M3, (d) M4.

Table 2. Main parameters and transport results by Elhakeem and Imran (2012) [53].

	1M1	2M1	3M1	4M1	5M1	6M1	7M1	8M1
θ'_* [-]	0.058	0.066	0.069	0.078	0.085	0.091	0.100	0.114
q [g/m/s]	4.24	14.37	18.98	27.05	47.89	57.81	103.63	123.23
d_{50} [mm]	2.03	1.95	1.98	2.04	2.26	2.49	2.66	2.50
	1M2	2M2	3M2	4M2	5M2	6M2	7M2	8M2
θ'_* [-]	0.058	0.072	0.092	0.101	0.113	0.121	0.131	0.144
q [g/m/s]	3.15	13.76	47.04	51.75	72.92	133.87	123.73	179.11
d_{50} [mm]	1.67	1.70	1.65	1.65	1.53	1.92	1.89	2.13
	1M3	2M3	3M3	4M3	5M3	6M3	7M3	8M3
θ'_* [-]	0.073	0.082	0.087	0.098	0.106	0.116	0.126	0.141
q [g/m/s]	8.52	22.48	26.52	34.82	60.46	69.63	137.55	151.90
d_{50} [mm]	1.36	1.18	1.36	4.27	4.45	4.94	5.04	5.45
	1M4	2M4	3M4	4M4	5M4	6M4	7M4	8M4
θ'_* [-]	0.060	0.076	0.077	0.084	0.095	0.110	0.131	0.156
q [g/m/s]	5.93	24.42	20.20	27.36	54.77	67.70	108.36	214.55
d_{50} [mm]	1.40	1.58	1.45	1.52	1.36	1.47	1.54	1.42

3. Theoretical Investigations

3.1. Transport Model for Non-Uniform Sediment

Following the work [50] for uniform sediments in steady flow and [51,52] for non-uniform sediments in the wave motion the multi-phase approach is used here because the different physical processes are responsible for sediment transport at various distances above an immobile bed. The specification of layers up to water surface elevation is proposed as follows (Figure 8): a dense layer (with immobile Coulomb friction sublayer and upper dense mobile sublayer dominated by grain collisions), a contact layer (where particle collisions and turbulent lift cooperate in momentum exchange) as well as a suspended sediment zone (which is divided into inner and outer flow regions). The inner flow region is characterized by a logarithmic velocity profile.

Under intensive hydrodynamic conditions with high grain mobility, the transport of sediment is characterized by very high concentration. It takes place at the entire layer of the dense mixture, in the form of a grain flow with a specific velocity $u_g(z')$ and concentration $c_g(z')$ profile. Under non-intensive conditions of low grain mobility, the dense layer is reduced to the upper sublayer, consisting of single grains being rolled and dragged over the bed surface, as in a typical bedload regime. Since both water and grains move in the mobile dense layer as well as in the layer of suspended sediment, there must be a transitional zone between these two regions, in which both velocity $u_i(z)$ and concentration $c_i(z)$ profiles of each fraction of the sediment mixture (Figure 8a) and the shear stress profile (Figure 8b) represent continuous shape. This transition zone is called the contact layer [47–50].

The presented model assumes that in the moving layer of densely concentrated sediments, all sediment fractions move at the velocity equal to the velocity of the mixture (at specified elevation). Hence, the interactions between the sediment fractions are assumed so strong, the finer fractions are slowed down by the thicker ones; all the fractions are characterized by the same velocity $u_g(z')$ and concentration $c_g(z')$ in vertical profiles. The model also takes into account, that the most intensive sorting of sediment occurs in the grain scattering process, in the contact layer and in turbulent flow region, which brings the sediment into suspension. In the contact layer, the vertical profiles of velocities $u_i(z)$ and concentrations $c_i(z)$ vary for individual fractions, due to turbulent fluid pulsations and chaotic collisions of grains.

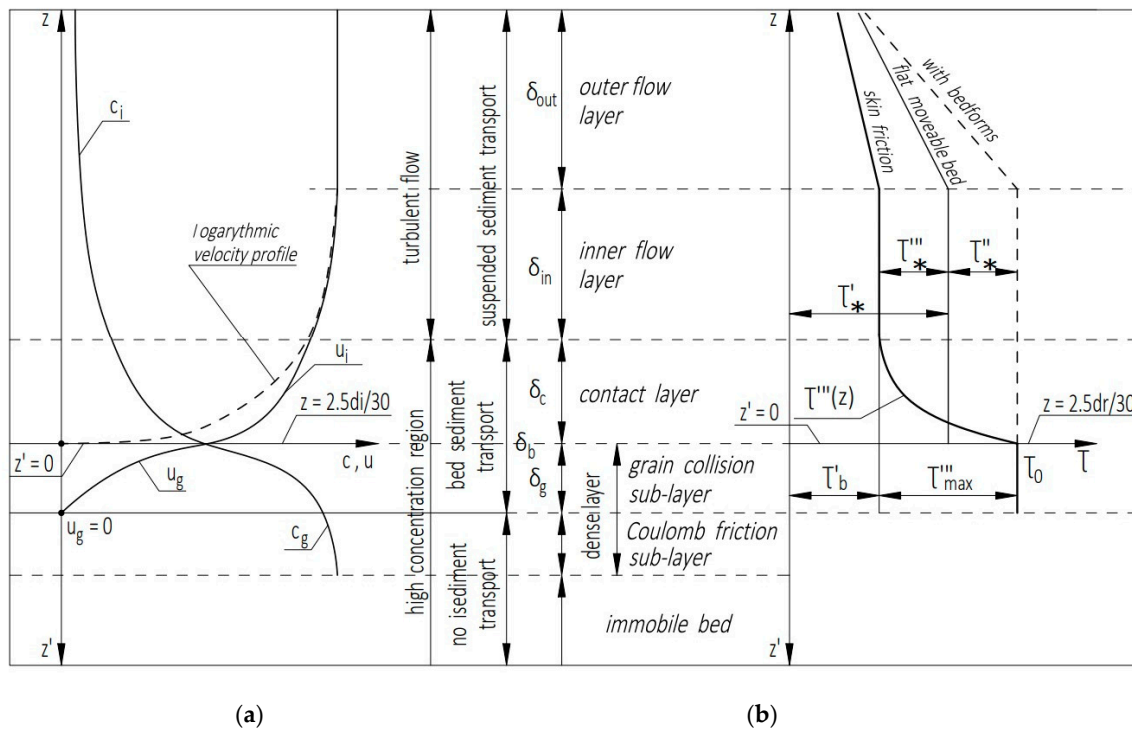


Figure 8. Vertical structure of: (a) sediment transport profile with velocity and concentration of the *i*-th fraction of sediment; (b) shear stress profile; after Kaczmarek et al. [50] with modification for non-uniform sediments.

The following mechanism of transmission of shear stress from the fluid to the immobile bed is proposed. The declining part of particle stresses, due to collisions of grains, in the upper dense sublayer is transferred directly to the moving grains. The increasing residual part, as the rate-independent component, is transferred further to the fixed bed. The concept of shear stress variation has been proposed originally by [50] for uniform sediments. Shear stress increases from the skin stress value τ'_b above the bed (Figure 8b) to the maximum value τ_0 at the bed, and then, the viscous part of this stress decays in the bed. The skin shear stress τ'_* above the bed, at the top of the contact layer, is identified as an input data with the value obtained from experiments. The skin shear stress τ'_* is the sum of bed skin friction τ'_b and drag friction τ''' due to motion of sediment particles, while τ''_* is the friction due to bed forms, when they are present.

Profiles of the velocity $u_g(z')$ and concentration $c_g(z')$ in the dense layer are calculated using the Equations (4) and (5) in a system of coordinates with the vertical axis z' directed downwards (Figure 8a):

$$\alpha^0 \left(\frac{c_g - c_0}{c_m - c_g} \right) \sin \varphi \sin 2\psi + \mu_1 \left(\frac{du_g}{dz'} \right)^2 = \tau_0, \tag{4}$$

$$\alpha^0 \left(\frac{c_g - c_0}{c_m - c_g} \right) (1 - \sin \varphi \cos 2\psi) + \mu_2 \left(\frac{du_g}{dz'} \right)^2 = \left(\frac{\mu_2}{\mu_1} \right) \Big|_{c_g=c_0} \tau_0 + (\rho_s - \rho) g \int_0^{z'} c_g dz', \tag{5}$$

where $\tau_0(t) = \rho u_{f0}^2(t)$; u_{f0} is the friction velocity at the top of the dense layer; $\alpha^0 = \text{constant} = \rho_s g d_r$; $c_m = 0.53$ is the maximum concentration of the bed sediment; $c_D = 0.32$ is the concentration of sediment at the upper limit of the dense layer; $\varphi = 24.4^\circ$ is the quasi-static angle of internal friction; $\psi =$ angle between the major principal stress and the horizontal axis:

$$\psi = \frac{\pi}{4} - \frac{\varphi}{2}, \tag{6}$$

$\mu_1, \mu_2 =$ functions of concentration, described [54] as

$$\mu_1 = \frac{0.03}{(c_m - c_g)^{1.5}} \rho_s d_r^2 \text{ and } \mu_2 = \frac{0.02}{(c_m - c_g)^{1.75}} \rho_s d_r^2. \tag{7}$$

The first component on the left-hand side of Equation (4) describes the shear stress relation for plastic stresses, while the second component represents “viscous” stresses. Similarly, the first element on the left-hand side of Equation (5) describes the normal stress relation for plastic stresses, while the second element describes normal “viscous” stresses. The combination of these stresses enables modelling both the declining part of grain collision stresses in the dense sublayer as well as the increasing residual part as the rate-independent component.

Assuming that settling of sediment balances the vertical exchange and the momentum exchange balances the shear stress, following [47,55], a set of two differential equations is proposed to determine the concentration and velocity profiles of the i -th sediment fraction in the contact layer:

$$\left[\frac{3}{2} \left(\alpha_s \frac{d_i}{w_s} \frac{du_i}{dz} \frac{3s + c_M}{2c_D} + \beta_i \right)^2 d_i^2 c_i^2 (s + c_M) + l^2 \right] \left(\frac{du_i}{dz} \right)^2 = u'_{f*}{}^2, \tag{8}$$

$$\left[3 \left(\alpha_s \frac{d_i}{w_{si}} \frac{du_i}{dz} \frac{2s + c_M}{3c_D} + \beta_i \right)^2 d_i^2 \frac{du_i}{dz} c_i + l^2 \frac{du_i}{dz} \right] \frac{dc_i}{dz} = -w_{si} c_i, \tag{9}$$

where vertical axis z is directed upward with the origin $z = \frac{k_s}{30}$ at the top of the dense layer; k_s is the skin roughness assumed as $k_s = 2.5d_i$; u'_{f*} is the skin shear velocity equal to $u'_{f*} = \sqrt{\frac{\tau'_0}{\rho}}$; d_i is the diameter of the i -th fraction; w_{si} = settling velocity of the i -th fraction; c_M = added hydrodynamic mass coefficient; $c_D = 1.0$ is a drag coefficient; l = mixing length equal to κz ; $(s + c_m)$ is assumed to be around value of 3.0. Coefficients $\alpha_i = \beta_i$ are calculated by the procedure which assumes the equality of the calculated sediment velocity $u_i(z)$ and the logarithmic flow velocity at the water surface elevation. The set of Equations (4) and (5) as well as Equations (8) and (9) are solved using numerical integration. The boundary conditions for a set of Equations (8) and (9) come from calculations in the dense layer with Equations (4) and (5) i.e., the velocity of sediment $u_g(z' = 0) = u_0$ corresponds to the concentration $c_0 = 0.32$.

Following the idea by [50] for uniform sediments, the mobile-bed effect parameter γ_0 is introduced:

$$\gamma_0 = \sqrt{\frac{\tau_0}{\tau'_*}} = \frac{u_{f0}}{u'_{f*}}, \tag{10}$$

In order to find the parameter γ_0 , it is assumed that bed sediment transport, calculated for both the dense and the contact layers (Figure 8), can be compared with a semi-empirical formula by MPM [13]. MPM formula is restricted to cases when the contribution of turbulent suspension load is negligible. Here, the MPM formula creates only a part of sediment transport, i.e., in the dense and contact layers. Hence, the formula described by Equation (11) seems to be a good option. Some other modifications of MPM formula, however, are possible when the data used for testing the model require the use of the MPM modifications.

According to the flow description shown in Figure 8, the following relationship can be postulated:

$$q_g \left(\rho \gamma_0^2 u_{f*}^2 \right) + q_c \left(\rho u_{f*}^2 \right) = \Phi_{MPM} \sqrt{(s - 1) g d_r^3}. \tag{11}$$

where sediment transport rate q_g in the grain collision sublayer (calculated by Equations (4) and (5)) is a shear stress function of $\rho\gamma_0^2 u_{f*}^2$ while sediment transport rate q_c in the contact layer is a function of shear stress of ρu_{f*}^2 and:

$$\Phi_{MPM} = 8(\theta'_* - \theta_c)^{1.5} \tag{12}$$

The parameter θ'_* defined in Equation (2) is called the Shields parameter, while the critical Shields parameter θ_c is a constant of the order of 0.05 for sand placed smoothly on a horizontal bed.

3.2. Model Results for Uniform Sediment

Figure 9 shows the results of calculations by presented model for uniform sediment of concentration in the contact layer (Figure 9a), and in grain collision sublayer (Figure 9b), as well as velocity in the contact layer (Figure 9c) and in grain collision sublayer (Figure 9d). Calculation results (solution of Equations (4) and (5) in grain collision sublayer and Equations (8) and (9) in contact layer) were obtained for the friction velocity $u_{f*} = 0.042$ m/s and for homogeneous sediment diameter ($d_r = d_i = d$) characterized by different grain diameters from $0.10 \text{ mm} \leq d \leq 2.97 \text{ mm}$. The calculations were performed for the sediment grain diameters from the measurements by Elhakeem and Imran [53].

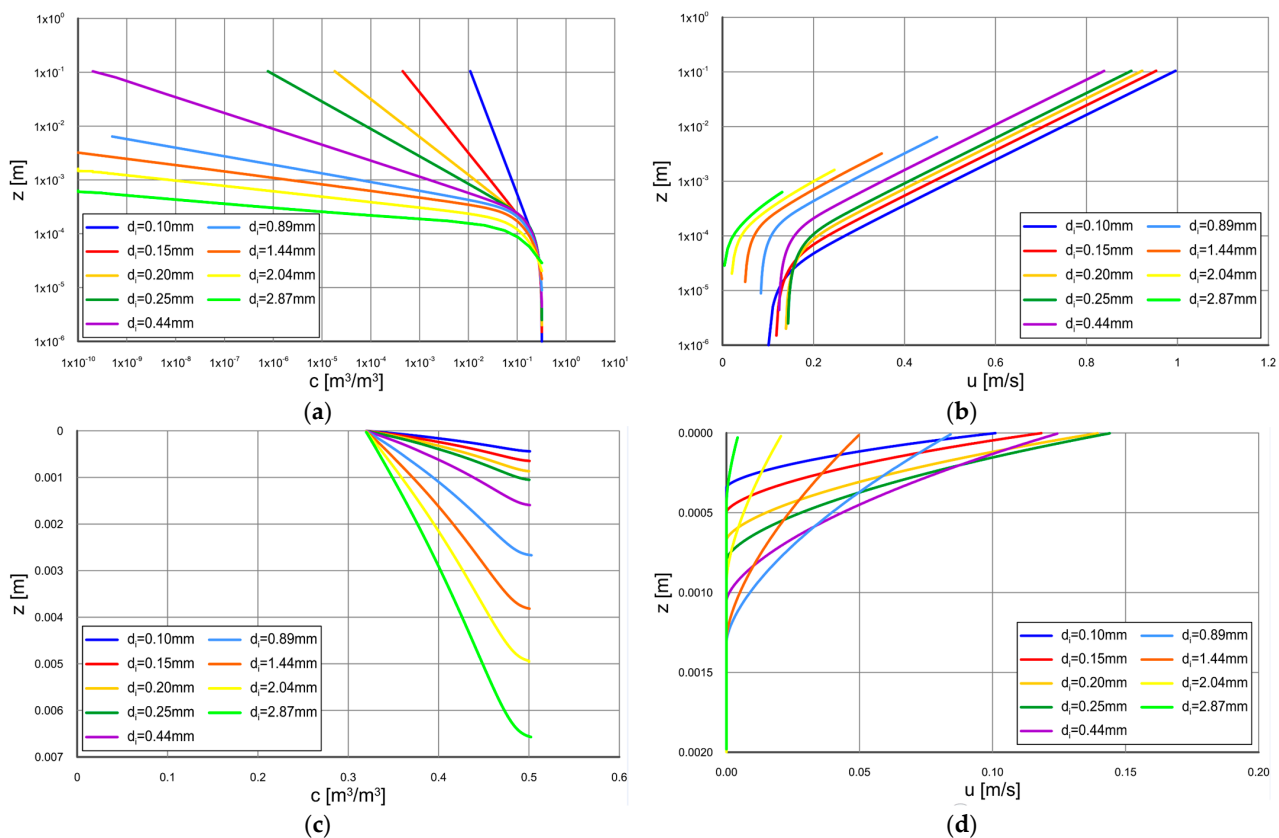


Figure 9. Calculated concentrations: (a) in the contact layer, (b) in grain collision sublayer and calculated velocities: (c) in the contact layer; (d) in grain collision sublayer for homogeneous sediments ($d_r = d_i$) and $u_{f*} = 0.042$ m/s.

In the Figure 9a,b it is seen that velocity and concentration vertical profiles reach the highest values in the contact layer for the smallest grain diameter ($d_i = 0.10$ mm), and gradually decrease with increasing diameter of the grains. All concentration profiles start with $c_0 = 0.32$ at the upper limit of dense layer. The velocity profiles, according to Figure 8,

start from the calculated value u_0 for coordinate $z_0 = k_s/30 = 2.5d_i/30$ which is set at this boundary. The z_0 ordinate increases with the grain diameter increase. It is worth noting that the velocity profile in the contact layer is connected to the logarithmic velocity profile at the upper boundary of this layer. The calculated logarithmic velocity distributions for the coarse fractions are stopped in Figure 8 at the levels where concentrations of these fractions reach negligibly small values.

Figure 9c shows that concentration in vertical profiles of coarse fractions reach their highest values at the distances from the upper limit of the grain collision sublayer greater than the distances for finer fractions. In other words, the larger the diameter of the grains, the greater the thickness of the collision sublayer (Figure 9c). Further, the velocities of finer fractions ($d < 0.25$ mm) increase with the increase in diameter and the thickness of the moving layer also increases, while velocities of coarser fractions ($d > 0.25$ mm) decrease with increasing diameter due to increasing resistance to motion.

3.3. Model Results for Non-Uniform Sediments

Coarser sediments in the mixture are more exposed to the flow, whereas finer sediments are hidden among the coarser ones. The hiding and exposure effects can affect the transport rates of sediment grain fractions. It is assumed in the model that all sediment fractions in the dense layer move at a velocity equal to the velocity of the mixture. Therefore, this assumption allows to take into account this effect in sediment transport calculations. In the dense layer all the fractions are characterized by the same vertical profile of velocity and concentration. Hence, more mobile fine fractions are slowed down by the thicker ones. It means that an increased amount of fine fractions in the bed results in consequent increase both in modeled velocity of the mixture and transport in the dense layer. In addition, the increased modeled velocity at the top of the dense layer results in increased modeled transport in the contact layer. Hence, the increase in coarse fractions in transport can occur even though their percentage contribution in the bed is reduced.

The above-mentioned effects are illustrated in Figure 10. Figure 10 shows the results of the model calculations of concentration (Figure 10a) and velocity (Figure 10c) in the contact layer, and concentration (Figure 10b) and velocity (Figure 10d) in grain—collision sublayer for heterogeneous sediments with a representative diameter d_r in the dense layer. It is clear that in the case of grains with the diameter d_i greater than d_r , the interaction between the fractions results in the increase in velocity at the upper limit of the dense layer, and leads to an increase in both the concentration value and the velocity of these fractions in the contact layer (Figure 10a,c) in relation to the relevant magnitudes for homogeneous sediments with $d_i = d_r$. In turn, in the case of grains with the diameter d_i smaller than the representative diameter d_r , the interaction between the fractions results in the reduction of velocity at the upper limit of the dense layer and leads to a decrease in both concentration and velocity in relation to the relevant magnitudes for homogeneous sediments. In grain—collision sublayer the movement of the mixture is determined by the representative diameter of d_r . Calculated profiles of velocity and concentration (Figure 10b,d) are the same as profiles for homogeneous sediments with diameters $d_i = d_r = 0.15$ mm, 1.9 mm and 2.87 mm.

Figure 11 presents the results of transport calculations of homogeneous sediments with different diameters of $d_i = d_r$ in the contact and grain—collision sublayers in comparison with transport calculations of sediment mixtures with different fractions d_i characterized by the representative diameters of $d_r = 0.2$ mm and 1.9 mm, respectively. It is obvious that the smaller the representative diameter d_r of the mixture, the greater the calculated transport values of all fractions. It is worth emphasizing that the calculated values of transport for diameters $d_i > d_r$ show an upward trend, with a significant increase in the case of mixtures with $d_r = 0.2$ mm. This increase is obviously due to the interaction between the fractions and the increase in velocities at the upper limit of the dense layer. In turn, transport calculations for the diameters $d_i < d_r$ show a decreasing trend with a significant decrease in the case of mixtures $d_r = 1.9$ mm. Finally, it is worth mentioning that the calculated transport for homogeneous sediments decreases to zero when the critical values $\theta_c = 0.05$.

This situation does not occur in mixtures when the values θ_c are not achieved under the given conditions ($u_{f*} = 0.042 \text{ m/s}$) for both diameters $d_r = 0.2 \text{ mm}$ and 1.9 mm .

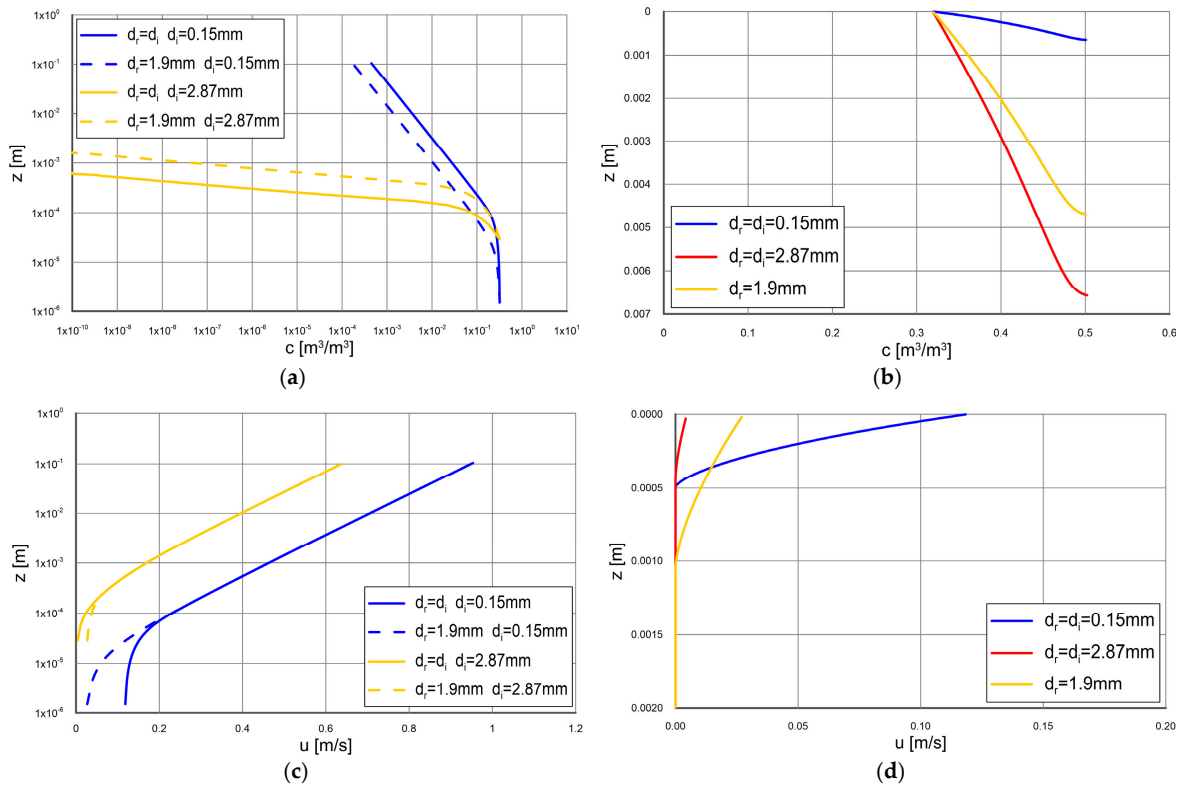


Figure 10. Calculation results ($u_{f*} = 0.042\text{m/s}$) of concentration in vertical profiles for heterogeneous sediments with the representative diameter d_r in: (a) the contact layer, (b) grain collision sublayer and of velocity vertical profile in: (c) the contact layer; (d) grain collision sublayer.

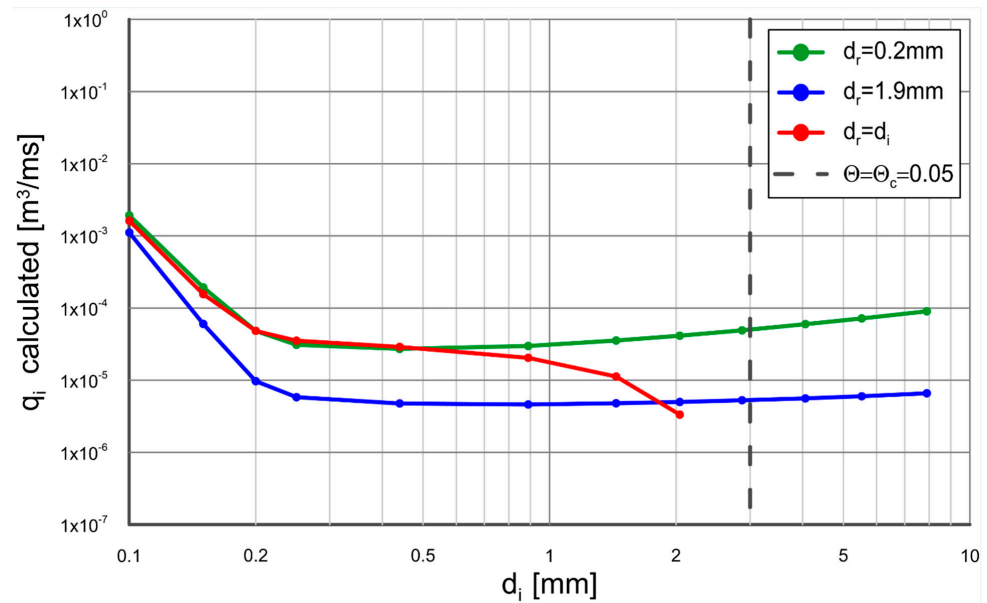


Figure 11. Exemplary result of calculations: the influence of fine fractions on transport of coarse fractions for $u_{f*} = 0.042 \text{ m/s}$.

4. Discussion

4.1. Non-Uniform Sediment Transport with Limited Availability of Very Fine Fractions

For the laboratory conditions bed level changes in the control volume i.e., the erosion rate in the box filled-up by sand is described by the continuity equation for sediment:

$$\frac{\partial h}{\partial t} = \frac{-\partial q}{(1-p)\partial x^-}, \quad (13)$$

where: h is the bed depth and sediment transport rate $q = \sum_{i=1}^N n_i q_i$ is calculated by presented model with the use of Equations (4) and (5) with the representative diameter of $d_r = d_{50}$ and Equations (8) and (9) with diameter d_i for the i -th sediment fraction, and Equations (11) and (12), while p is the sediment porosity, assumed as 0.4. The amount $\frac{\partial q}{\partial x^-}$ means the directional derivative in the x^- direction. In the further part of this paper the term $(1-p)$ will be omitted. Although it should be remembered that in order to obtain the actual thickness value, the calculated values of these quantities should be divided by the $(1-p)$ term.

From the finite difference scheme, one obtains the thickness of the layer Δh which is eroded in time Δt with transport rate q along the distance Δx :

$$\Delta h = \frac{\Delta t}{\Delta x} q. \quad (14)$$

Similarly, the thickness of the eroded layer can be determined for each i -th fraction:

$$n_i \Delta h_i = \frac{\Delta t}{\Delta x} n_i q_i, \quad (15)$$

because

$$\Delta h = \sum_{i=1}^N n_i \Delta h_i, \quad (16)$$

and bearing in mind that each value Δh_i is related to the contribution of each fraction n_i (with $\sum n_i = 1$), the following formula for the new contribution of each fraction m_i at the considered location of erosion is proposed:

$$m_i = \frac{n_i h_m - n_i \Delta h_i}{h_m - \Delta h} = \frac{n_i h_m - \frac{\Delta t}{\Delta x} n_i q_i}{h_m - \sum_{i=1}^N n_i \Delta h_i}, \quad (17)$$

which satisfies the condition $\sum m_i = 1$. In Equation (17) h_m denotes the thickness of the "mixing" or "active", layer, i.e., the thickness of the sediment layer in which the contribution of the grain size fraction changes from n_i to m_i in time Δt . This change takes place due to sand transport rate q at the distance Δx . The first term on the right-hand side of Equation (17) is related with the availability of the i -th fraction, while the second term is related with the erosion rate at the considered location.

An important question concerns the value of the "mixing" layer thickness h_m . Following [45] it can be proposed:

$$h_m = 2 \frac{\Delta t}{\Delta x} \sum_{i=1}^N n_i q_i, \quad (18)$$

The above implies that about half of the sand is conducted from the analyzed location, while the other half is subject to mixing and remains at this location. The above statement is confirmed in experimental studies shown by [47]. It can be noted from the form of Equations (15), (17) and (18) that the ratio $\Delta t / \Delta x$ is present in all terms of the numerator and denominator of Equation (17) and therefore disappears. Hence, the new grain size distribution inside the mixing layer, calculated from Equation (17), does not depend on time and space discretization. However, based on, Equation (18) the layer with the new

grain size distribution increases in time, up to an ultimate value h_m after time Δt . The mixing layer thickness h_m is an important physical quantity and should be known.

Hence, for known value of the mixing layer thickness h_m one can assess the time Δt_k necessary for formation of the sediment layer sometimes called “carpet layer”, sorted over the thickness a^* . From Equation (18) it is obtained:

$$\Delta t_k = \frac{h_m \Delta x}{2 \sum_{i=1}^N n_i q_i}, \tag{19}$$

The condition of the availability of each fraction of the sediment should fulfill the form:

$$h_m \geq \frac{\Delta t_k}{\Delta x} q_i, \tag{20}$$

If the availability of the i -th fraction of sediment is limited (condition Equation (21) is not complied), then the sediment transport rate of the i -th fraction is reduced from the value q_i to the value:

$$q_i^n = \frac{h_m \Delta x}{\Delta t_k}, \tag{21}$$

where

$$\Delta h_i^n = \frac{\Delta t}{\Delta x} q_i^n. \tag{22}$$

The changes of grain sizes inside the carpet layer after time Δt can be determined as follows:

$$m_i = \frac{n_i h_m - n_i \Delta h_i}{h_m - \sum_{i=1}^N \Delta h_i} = \frac{n_i h_m - \frac{\Delta t}{\Delta x} n_i q_i^n}{h_m - \sum_{i=1}^N \frac{\Delta t}{\Delta x} n_i q_i^n}. \tag{23}$$

In case the condition (20) is not complied for the i -th fraction then its contribution to grain size distribution inside the carpet a^* after time Δt_k is $m_i = 0$. The grain size distribution inside the mixing layer of the thickness h_m after time Δt_k will thus be determined by Equation (23), as well as by smaller contribution of the source (input) sediment n_{si} in the form:

$$n_i^n = \frac{a m_i + (h_m - a^*) n_{si}}{h_m}, \tag{24}$$

where:

$$a^* = h_m - \sum_{i=1}^N \frac{\Delta t_k}{\Delta x} q_i, \tag{25}$$

is calculated for q_i or q_i^n if it is required.

The calculation procedure is repeated using Equations (19)–(25) with $n_i = n_i^n$ in each time step k . Finally, the reduced transport rate after time $\Delta t = \sum_{k=1}^K \Delta t_k$ of the i -th very fine fraction is calculated as follows:

$$q_i^n = \frac{\sum_{k=1}^K (q_i^n)_k \cdot \Delta t_k}{\Delta t}. \tag{26}$$

where: K is the number of steps, Δt_k is time interval in each step, calculated according to the Equation (19) for n_i^n and q_i or q_i^n , if required.

Finally, it is worth mentioning that a constant value of the representative diameter $d_r = d_{50}$ in the dense layer is assumed, despite the changes in grain size during that time. As the recent studies on the sediment fluxes during the crest of the wave [36,37] have shown such changes lead to an increase in the roughness of the bottom and may have an impact on reducing sediment transport. It seems, however, that in the laboratory Gdańsk 2021 conditions for steady flow, the major reduction of sediment transport is due to a possible deficit of fine fractions in the bed.

Figure 12 presents the results of calculations of the thickness of the bottom erosion caused by the transport of q_i of the i -th sediment fraction with diameter d_i . Calculations

of Δh_i were conducted for a case without taking into account the limited availability of individual fractions in the bed. Calculations for the thickness of Δh_i^n were obtained for a case when the reduction of transport to the values q_i^n due to deficit of a given fraction was taken into account. From Figure 12 it can be seen that the availability of at least two fractions was limited and there was a significant reduction of both the transport of these fractions from q_i to q_i^n as well as the thickness of erosion caused by this transport from Δh_i to Δh_i^n . It is worth noting that the quantities q_i^n were averaged according to the Equation (26), while the quantities Δh_i^n according to the formula:

$$\Delta h_i^n = \frac{\sum_{k=1}^K (\Delta h_i^n)_k \cdot \Delta t_k}{\Delta t} \tag{27}$$

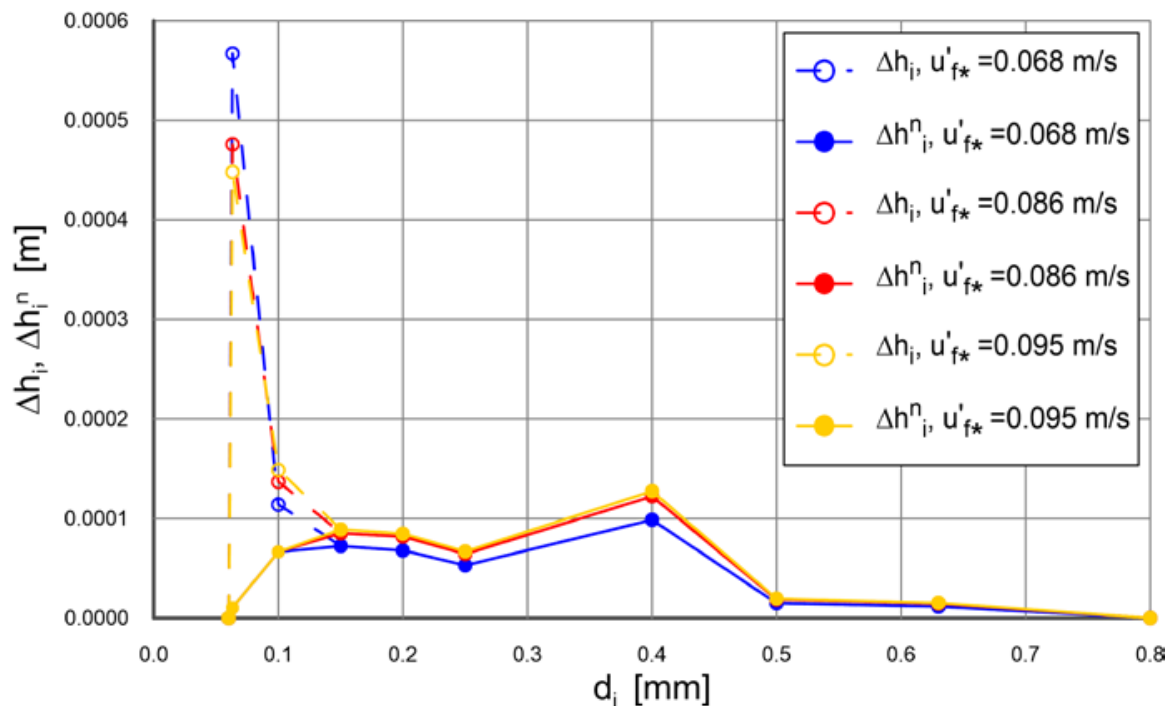


Figure 12. Model results of the erosion thickness Δh_i of the i -th sediment fraction caused by transport q_i and the reduced thickness Δh_i^n caused by q_i^n due to limited availability of very fine fractions.

4.2. Comparison Calculations with Measurements

4.2.1. Experiment Gdańsk 2021

In Figure 13 the results of transport calculations compared to the results of experiment Gdańsk 2021 are presented. The calculations were made using the presented model [48] with the proposed modification taking into account the deficit of very fine fractions in the mixing layer in the bottom. The calculations were conducted, both for transport of all fractions and for transport of fine fractions, defined as:

$$(q_f)_{calc} = \sum_{i=1}^{N_f} (q_i^n)_{calc} \tag{28}$$

where $i = N_f$ means fraction with a diameter of $d_i = 0.2$ mm. Transport of coarse fractions is defined as:

$$(q_c)_{calc} = \sum_{i=N_f}^N (q_i)_{calc} \tag{29}$$

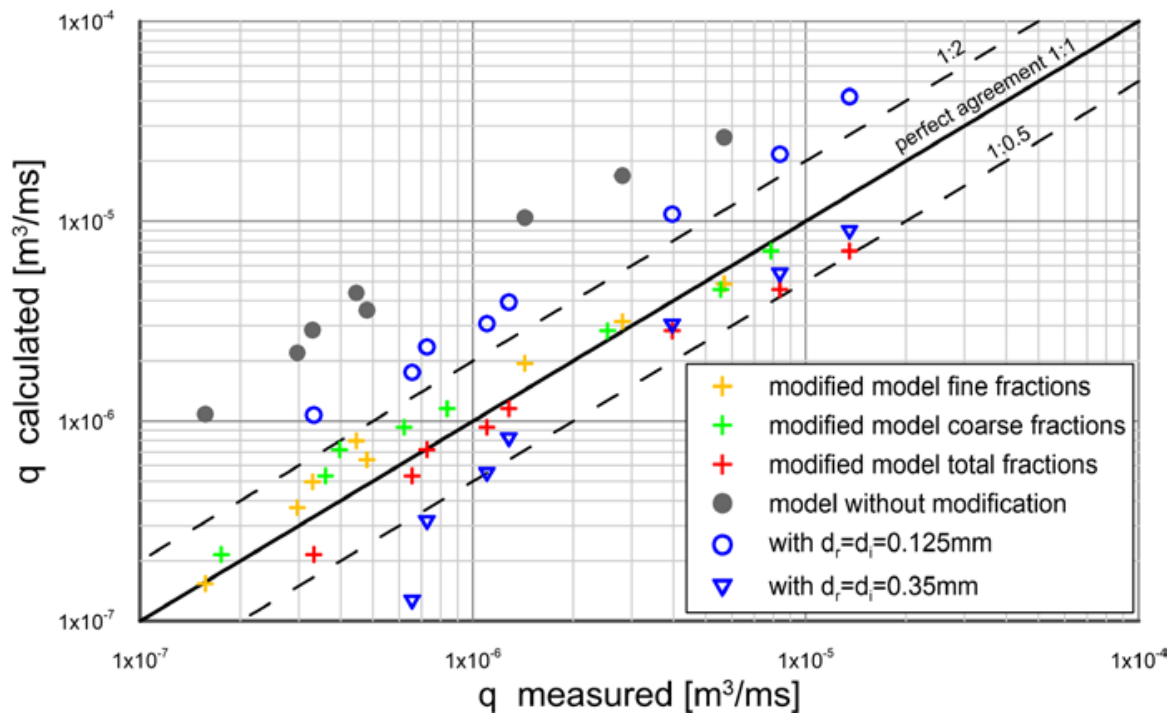


Figure 13. Comparison of sediment transport calculations with modification due to very fine fraction deficit, with calculations without modification, and with calculations for uniform sediments ($d_r = d_i = 0.125$ mm and $d_r = d_i = 0.35$ mm).

The values calculated with the Equations (28) and (29) were compared with the measured values $q_{meas.}$, which are the mean values of measurement ‘TR tests’:

$$(q_f)_{meas} = \sum_{i=N_f}^N q_{meas.} (n_{fi})_{meas} , \tag{30}$$

$$(q_c)_{meas} = \sum_{i=N_f}^N q_{meas.} (n_{ci})_{meas} , \tag{31}$$

where: $n_{fi_{meas.}}$ —contribution of the i -th fine and very fine fraction ($d_i < 0.2$ mm) in the mixture collected from the trap, $n_{ci_{meas.}}$ —contribution of the i -th coarse fraction ($d_i \geq 0.2$ mm) in the mixture collected from the trap.

Figure 13 shows the agreement of the results of calculations taking into account the deficit of very fine fractions with the measurements is within plus/minus a factor of 2. Figure 13 also shows the results of calculations without modification due to the deficit of very fine fractions. In addition, the results of calculations by presented model for uniform sediment with $d_r = d_i = 0.125$ mm and $d_r = d_i = 0.35$ mm are shown in Figure 13. As expected, in these cases a worse compatibility of the results was obtained, especially of the results for non-uniform sediment without modification due to very fine fraction deficit. This confirms the lack of full availability of very fine fractions in the bottom is the main reason for a significant reduction in transport of those fractions. Note that the over-predictions of the model for uniform sediment with $d_r = d_i = 0.125$ mm is much smaller than for non-uniform sediment without modification due to very fine fraction deficit.

In turn, a very good compliance of the transport calculations when this deficit is taking into account allows expecting very good compliance of the calculation results of the share of fine and very fine fractions with the measured grain size distribution. A comparison of the calculation results of the grain size distribution of sediments caught in the trap with the

measurements is presented in the Figure 14. Figure 14 shows a consistency of the results was obtained within plus/minus a factor of two of the measurements.

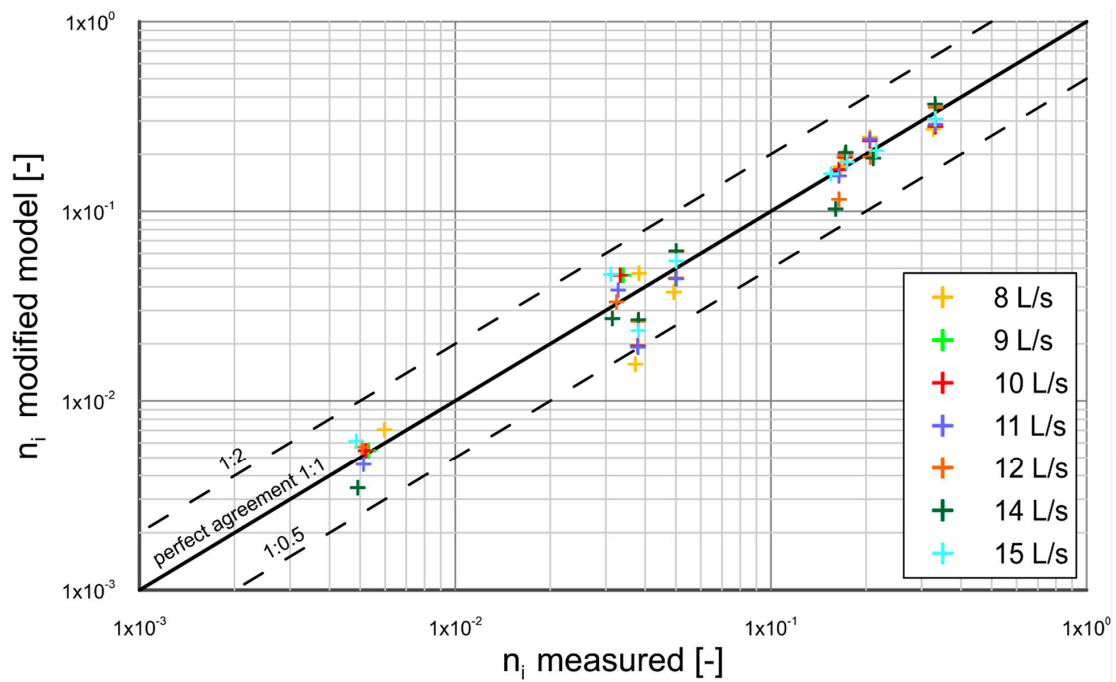


Figure 14. Comparison of grain size distribution calculations by presented model with modification for limited availability of fine fractions with measurements Gdańsk 2021.

Finally, it is worth noting the results of transport calculations (Figure 15) approximated by linear curve $y = ax$ with a coefficient of determination R^2 . As it is seen, a high value of fit is obtained and the deviation of the correlation curve from $y = x$ is negligibly small.

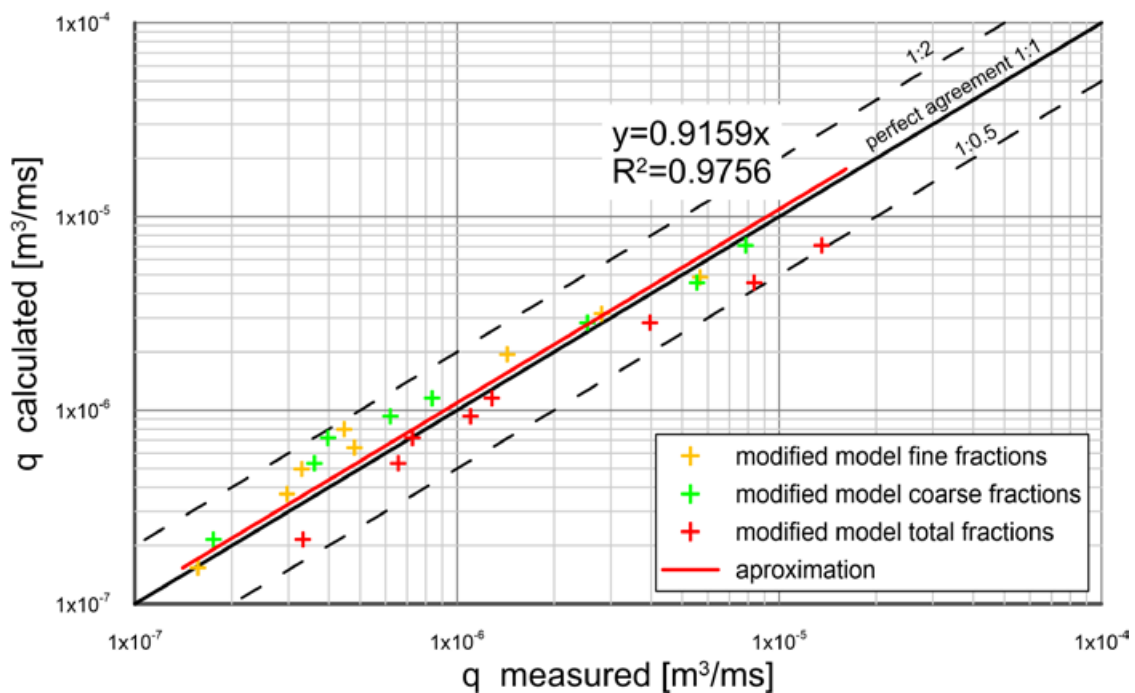


Figure 15. Transport calculations for Gdańsk 2021 data, approximated by linear curve $y = ax$ with a coefficient of determination R^2 .

4.2.2. Experiment by Elhakeem and Imran [53]

In the Figure 16 the results of transport calculations are compared to the results of experimental studies by [53]. The calculations were made using presented model for four initial distributions of the M1–M4 grain size. Again, the agreement of sediment transport calculations with measurements have been achieved within plus/minus a factor of two of the measurements. This confirms that the mechanism of interactions between fractions, and in particular the influence of finer grains in the mixture on the increase in the transport of coarse fractions, is well described by presented model.

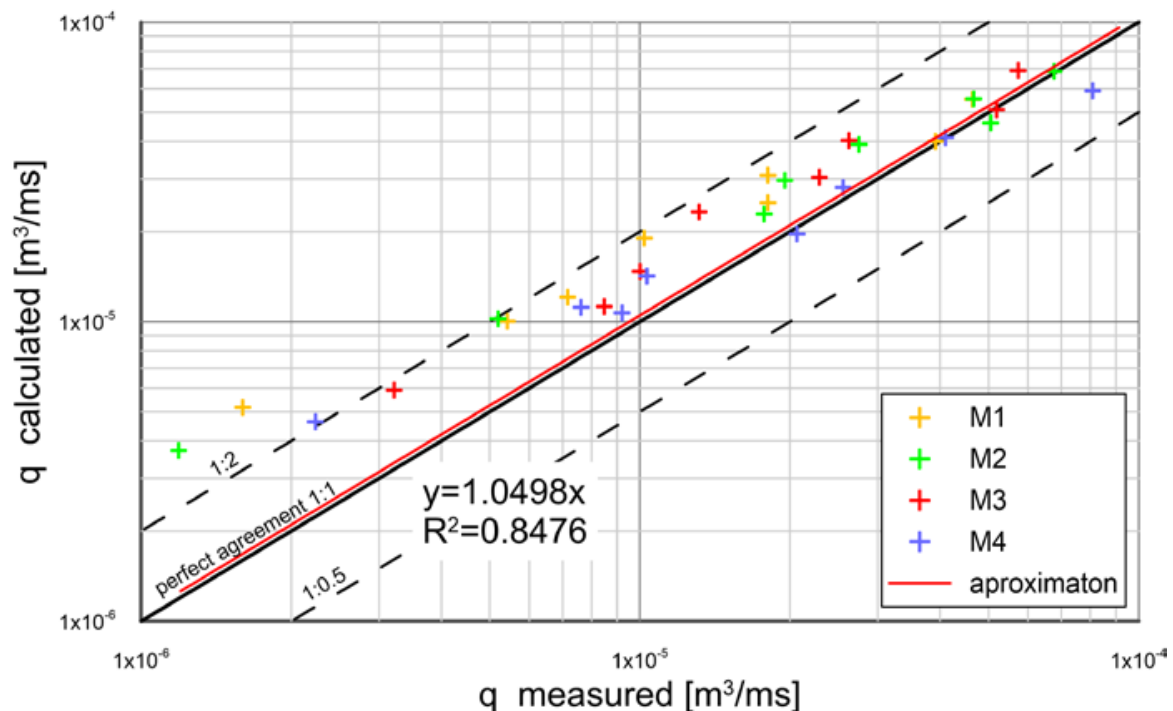


Figure 16. Transport calculations for the data by [53] approximated by curve $y = ax$ with a coefficient of determination R^2 .

The results of transport calculations were approximated by a straight linear $y = ax$ with a coefficient of determination R^2 (Figure 16). Again, a high value of fit is obtained and the deviation of the correlation line $y = x$ is very small. However, some small over-predictions in the lower transport regime are evident. This effect is in accordance with the estimations made by Wong and Parker [56] in lower regime of bedload transport rates which were less than or equal to half the values that would be obtained with the original MPM formula. At this moment, there are too small amount of experimental data and thus it is very difficult to decide whether use MPM modifications or not.

In addition, a comparison of the calculations of the grain size distributions of sediments from the trap with the measurements for all initial grain size distributions (M1–M4) presented in Figure 17 shows that the results are consistent with measurements within plus/minus a factor of two.

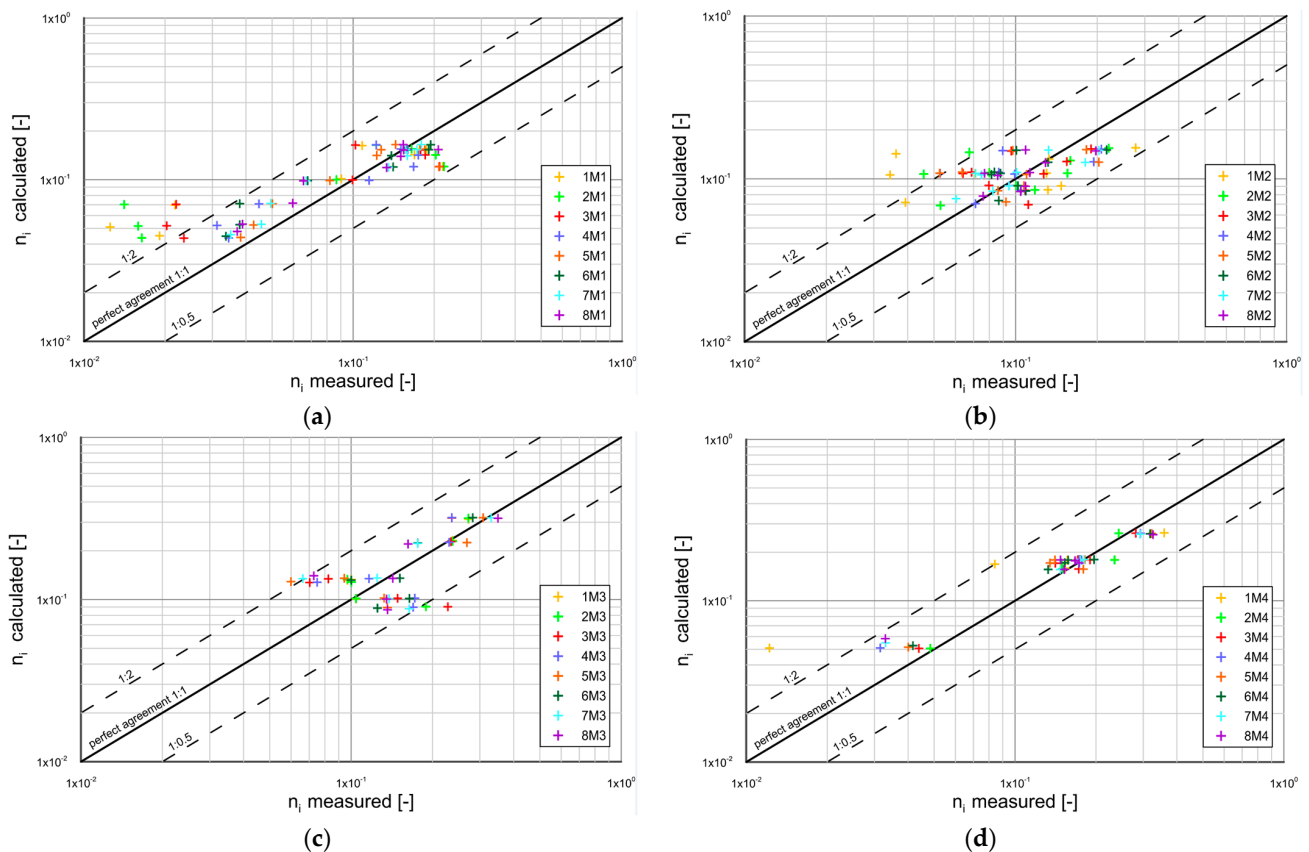


Figure 17. Comparison of grain size distribution calculations with measurements by [53] for: initial grain size distribution: (a) M1, (b) M2, (c) M3 and (d) M4.

5. Conclusions

Theoretical and experimental studies conducted on transport of sediment mixtures in steady flow allowed us to draw the following conclusions:

- Transport calculations conducted by the presented model separately for all sediment fractions in mixture including the mutual interactions between them have shown:
 - due to assumed strong interactions between the sediment fractions in the moving layer of densely concentrated sediments all the fractions are characterized by the same velocity and concentration vertical profiles;
 - in the contact layer vertical profiles of velocities and concentrations vary for individual fractions due to turbulent water pulsations and chaotic collisions of grains;
 - the agreement between the calculated transport and measurements was achieved within plus/minus a factor of two of the measurements;
 - calculations of the granulometric distributions of sediment from the trap conducted using presented model have shown good agreement with the measurements (plus/minus a factor of two of the measurements);
 - results confirm that the mechanism of interactions between fractions, and in particular the influence of finer grains in the mixture on the increase in transport of coarser fractions, is well described by the model.
- The experimental investigations on transport of sediment mixture with large amount of very fine non-cohesive fractions resulted in proposed modification by inclusion of possible deficit of very small fractions in the active layer of the bottom. The compatibility of the transport calculation results for all fractions with measurements Gdańsk 2021 is within plus/minus a factor of two of the measurements. This confirms

the lack of full availability of very fine fractions in the bottom and be the reason for a significant reduction in transport of those fractions.

3. Comparison of the calculations by presented modified model of grain size distributions with measurements Gdańsk 2021 shows consistency with the experimental results within plus/minus a factor of two of the measurements.
4. The presented study provides verified three-layer model which enables the proper description of sediment transport and grain size distributions of transported fractions in steady flow for any bed sediment mixtures, including poorly and well sorted grains with large amount of very fine non-cohesive fractions.
5. The present study provides a useful engineering tool for prediction of transport in steady flow of sediment mixtures with various non-cohesive fractions including very fine and fine. Calculations are possible with just a few measurable properties of particles and water. Parameters do not need tuning against experiments.
6. The next step of model development will be the extension to transport modeling in steady flow of sand mixtures with cohesive admixtures. The authors look forward to work also on model extension to predict sediment transport under highly transient (e.g., dam-break) flows.

Author Contributions: Conceptualization, J.Z. and L.M.K.; methodology, J.Z., L.M.K. and J.B.; formal analysis, J.Z., L.M.K., J.B. and I.R.; investigation, J.Z., L.M.K., J.B. and I.R.; resources, L.M.K.; writing—original draft preparation, J.Z. and L.M.K.; writing—review and editing, J.Z., L.M.K. and I.R.; supervision, L.M.K.; project administration, J.Z. and L.M.K.; funding acquisition, J.Z. and L.M.K. All authors have read and agreed to the published version of the manuscript.

Funding: The research was financially supported by “ZINTEGROWANI- Kompleksowy Program Rozwoju Politechniki Koszalińskiej” nr POWR.03.05.00-00-Z055/18: Projekt współfinansowany ze środków Unii Europejskiej z Europejskiego Funduszu Społecznego w ramach Programu Operacyjnego Wiedza Edukacja Rozwój 2014–2020 and the research project of the Koszalin University of Technology, Faculty of Civil Engineering, Environmental and Geodetic Sciences: Dynamika niespoistego, niejednorodnego granulometrycznie ośrodka gruntowego w przepływie stacjonarnym i ruchu falowym w warunkach silnie nachylonego dna—funds no.: 524.01.07; project manager: L.K.

Institutional Review Board Statement: Not applicable.

Informed Consent Statement: Not applicable.

Data Availability Statement: The data presented in this study are available upon request from the corresponding author.

Conflicts of Interest: The authors declare no conflict of interest.

References

1. Mc Laren, P.; Bowles, D. The Effects of Sediment Transport on Grain-Size Distributions. *J. Sediment. Res.* **1985**, *55*, 457–470.
2. Van Rijn, L.C. *Longshore sediment transport, Report Z3054*; Delft Hydraulics: Delft, The Netherlands, 2001.
3. Van Rijn, L.C. Unified View of Sediment Transport by Currents and Waves. I: Initiation of Motion, Bed Roughness, and Bed-Load Transport. *J. Hydraul. Eng.* **2007**, *133*, 649–667. [[CrossRef](#)]
4. Van Rijn, L.C. Unified View of Sediment Transport by Currents and Waves. II: Suspended Transport. *J. Hydraul. Eng.* **2007**, *133*, 668–689. [[CrossRef](#)]
5. Van Rijn, L.C. Unified View of Sediment Transport by Currents and Waves. III: Graded Beds. *J. Hydraul. Eng.* **2007**, *133*, 761–775. [[CrossRef](#)]
6. Van Rijn, L.C.; Walstra, D.J.R.; van Ormondt, M. Unified view of sediment transport by currents and waves. IV: Application of morpho dynamic model. *J. Hydraul. Eng.* **2007**, *133*, 776–793. [[CrossRef](#)]
7. Van Rijn, L.C.; Grasmeyer, B.T.; Perk, L. Effect of channel deepening on tidal flow and sediment transport, part 1. Sandy channels. *Ocean Dyn.* **2018**, *68*, 1457–1479. [[CrossRef](#)]
8. Egiazaroff, I.V. Calculation of nonuniform sediment concentrations. *J. Hydraul. Div.* **1965**, *91*, 225–247. [[CrossRef](#)]
9. Gessler, J. Beginning and ceasing sediment motion. In *River Mechanics*; Shen, H.W., Ed.; Water Resources: Littleton, CO, USA, 1971; Chapter 7.
10. Parker, G.; Klingeman, P.C. On why gravel bed streams are paved. *Water Resour. Res.* **1982**, *18*, 1409–1423. [[CrossRef](#)]
11. Wilcock, P.R.; Mc Ardell, B.W. Surface-based fractional transport rates: Mobilization thresholds and partial transport of a sand-gravel sediment. *Water Resour. Res.* **1993**, *29*, 1297–1312. [[CrossRef](#)]

12. Paola, C.; Seal, R. Grain Size Patchiness as a Cause of Selective Deposition and Downstream Fining. *Water Resour. Res.* **1995**, *31*, 1395–1407. [[CrossRef](#)]
13. Meyer-Peter, E.; Müller, R. Formulas for bed-load transport. In Proceedings of the 2nd Meeting of the International Association for Hydraulic Structures Research, Delft, The Netherlands, 7 June 1948; International IAHR Congress. International Association for Hydro-Environment Engineering and Research: Stockholm, Sweden, 1948.
14. Mc Carrona, C.J.; Van Landeghema, K.J.J.; Baasa, J.H.; Amoudryb, L.O.; Malarkey, J. The hiding-exposure effect revisited: A method to calculate the mobility of bimodal sediment mixtures. *Mar. Geol.* **2019**, *410*, 22–31. [[CrossRef](#)]
15. Khosravi, K.; Chegini, A.H.N.; Mao, L.; Rodriguez, J.F.; Saco, P.M.; Binns, A.D. Experimental Analysis of Incipient Motion for Uniform and Graded Sediments. *Water* **2021**, *13*, 1874. [[CrossRef](#)]
16. Dey, S.; Ravi Kishore, G.; Castro-Orgaz, O.; Ali, S.Z. Hydrodynamics of submerged turbulent plane offset jets. *Phys. Fluids* **2017**, *29*, 065112. [[CrossRef](#)]
17. Ancey, C. Stochastic modeling in sediment dynamics: Exner equation for planar bed incipient bed load transport conditions. *J. Geo-Phys. Res.* **2010**, *115*, F00A11. [[CrossRef](#)]
18. Furbish, D.J.; Haff, P.K.; Roseberry, J.C.; Schmeckle, M.W. A probabilistic description of the bed load sediment flux: 1. Theory. *J. Geo-Phys. Res. Earth Surf.* **2012**, *117*, F03031. [[CrossRef](#)]
19. Heyman, J.; Ma, H.B.; Mettra, F.; Ancey, C. Spatial correlations in bed load transport: Evidence, importance, and modelling. *J. Geo-Phys. Res. Earth Surf.* **2014**, *119*, 1751–1767. [[CrossRef](#)]
20. Bialik, R.J.; Nikora, V.I.; Rowiński, P.M. 3D Lagrangian modeling of saltating particles diffusion in turbulent water flow. *Acta Geophys.* **2012**, *60*, 1639–1660. [[CrossRef](#)]
21. Nikora, V.I.; Rowiński, P.M. Rough-bed flows in geophysical, environmental, and engineering systems: Double-Averaging Approach and its applications. *Acta Geophys.* **2008**, *56*, 529–533. [[CrossRef](#)]
22. Vowinkel, B.; Nikora, V.; Kempe, T.; Fröhlich, J. Momentum balance in flows over mobile granular beds: Application of double averaging methodology to DNS data. *J. Hydraul. Res.* **2017**, *55*, 190–207. [[CrossRef](#)]
23. Vowinkel, B.; Nikora, V.; Kempe, T.; Fröhlich, J. Spatially averaged momentum fluxes and stresses in flows over mobile granular beds: A DNS-based study. *J. Hydraul. Res.* **2017**, *55*, 208–223. [[CrossRef](#)]
24. Berzi, D.; Fraccarollo, L. Intense sediment transport: Collisional to turbulent suspension. *Phys. Fluids* **2016**, *28*, 023302. [[CrossRef](#)]
25. Jenkins, J.T.; Hanes, D.M. Collisional sheet flows of sediment driven by a turbulent fluid. *J. Fluid Mech.* **1998**, *370*, 29–52. [[CrossRef](#)]
26. Pasini, J.M.; Jenkins, J.T. Aeolian transport with collisional suspension. *Phil. Trans. R. Soc. A.* **2005**, *363*, 1625–1646. [[CrossRef](#)] [[PubMed](#)]
27. Graf, W.H. *Hydraulics of Sediment Transport*; McGraw-Hill: New York, NY, USA, 1971.
28. Vanoni, V.A. *Sedimentation Engineering Practice*. American Society of Civil Engineers. In *Manuals and Reports on Engineering Practice*; American Society of Civil Engineers: Reston, VA, USA, 1975; Volume 54, 745p.
29. Yalin, M.S. *Mechanics of Sediment Transport*; Pergamon Press: London, UK, 1977.
30. Sharma, A.; Kumar, B. Flow structure over uniform and nonuniform sand bed channel E. In Proceedings of the 38th IAHR World Congress, Panama City, Panama, 1–6 September 2019. [[CrossRef](#)]
31. Sahoo, A.; Samantaray, S.; Singh, R.B. Analysis of Velocity Profiles in Rectangular Straight Open Channel Flow. *Pertanika J. Sci. Technol.* **2020**, *28*, 1–18.
32. Cheng, C.H.; de Smit, J.C.; Fivash, G.S.; Hulscher, S.J.M.H.; Borsje, B.W.; Soetaert, K. Sediment shell-content diminishes current-driven sand ripple development and migration. *Earth Surf. Dynam.* **2021**, *9*, 1335–1346. [[CrossRef](#)]
33. Sleath, J.F.A. *Sea Bed Mechanics (Ocean Engineering)*; John Wiley and Sons Inc.: Chichester, UK, 1984; ISBN 9780471890911.
34. Nielsen, P. *Coastal Bottom Boundary Layers and Sediment Transport*; Advanced Series on Ocean Engineering; World Scientific: Singapore, 1992; Volume 4.
35. Fredsøe, J.; Deigaard, R. *Mechanics of Coastal Sediment Transport*; Advanced Series on Ocean Engineering; World Scientific: Singapore, 1992; Volume 3.
36. Soulsby, R. *Dynamics of Marine Sands: A Manual for Practical Applications*; Thomas Telford: London, UK, 1997.
37. Selim, T.; Hesham, M.; Elkiki, M. Effect of sediment transport on flow characteristics in non-prismatic compound channels. *Ain Shams Eng. J.* **2022**, *13*, 101771. [[CrossRef](#)]
38. Miller, M.C.; Mc Cave, I.N.; Komar, P.D. Threshold of sediment motion under unidirectional currents. *Sedimentology* **1977**, *24*, 507–527. [[CrossRef](#)]
39. Thorn, M. Coastal and estuarine sediment dynamics by K.R. Dyer. Wiley, Chichester. *Geol. J.* **1987**, *22*, 169. [[CrossRef](#)]
40. Voulgaris, G.; Wallbridge, S.; Tomlinson, B.N.; Collins, M.B. Laboratory investigations into wave period effects on sand bed erodibility under the combined action of waves and currents. *Coastal Eng.* **1995**, *26*, 117–134. [[CrossRef](#)]
41. Sharma, A.; Kumar, B. Comparison of Flow and Morphological Characteristics in Uniform and Non-uniform Sand Bed Channel. *Can. J. Civ. Eng.* **2020**, *47*, 678–690. [[CrossRef](#)]
42. Stone, M.; Krishnappan, B.G.; Silins, U.; Emelko, M.B.; Williams, C.H.S.; Collins, A.L.; Spencer, S.A. A New Framework for Modelling Fine Sediment Transport in Rivers Includes Flocculation to Inform Reservoir Management in Wildfire Impacted Watersheds. *Water* **2021**, *13*, 2319. [[CrossRef](#)]
43. Wilcock, P.R.; Kenworthy, S.T.; Crowe, J.C. Experimental study of the transport of mixed sand and gravel. *Water Resour. Res.* **2001**, *37*, 3349–3358. [[CrossRef](#)]

44. Radosz, I.; Zawisza, J.; Biegowski, J.; Paprota, M.; Majewski, D.; Kaczmarek, L.M. An Experimental Study on Progressive and Reverse Fluxes of Sediments with Fine Fractions in Wave Motion. *Water* **2022**, *14*, 2397. [[CrossRef](#)]
45. Radosz, I.; Zawisza, J.; Biegowski, J.; Paprota, M.; Majewski, D.; Kaczmarek, L.M. An Experimental Study on Progressive and Reverse Fluxes of Sediments with Fine Fractions in the Wave Motion over Sloped Bed. *Water* **2023**, *15*, 125. [[CrossRef](#)]
46. Kaczmarek, L.M. *Moveable Sea Bed Boundary Layer and Mechanics of Sediment Transport*; Institute of Hydroengineering of the Polish Academy of Sciences: Gdańsk, Poland, 1999.
47. Kaczmarek, L.M.; Biegowski, J.; Ostrowski, R. Modelling cross-shore intensive sand transport and changes of bed grain size distribution versus field data. *Coastal Eng.* **2004**, *51*, 501–529. [[CrossRef](#)]
48. Kaczmarek, L.M.; Sawczyński, S.; Biegowski, J. Hydrodynamic equilibrium for sediment transport and bed response to wave motion. *Acta Geophys.* **2015**, *63*, 486–513. [[CrossRef](#)]
49. Kaczmarek, L.M.; Sawczyński, S.; Biegowski, J. An equilibrium transport formula for modeling sedimentation of dredged channels. *Coastal Eng. J.* **2017**, *59*, 1750015-1. [[CrossRef](#)]
50. Kaczmarek, L.M.; Biegowski, J.; Sobczak, Ł. Modeling of Sediment Transport in Steady Flow over Mobile Granular Bed. *J. Hydraul. Eng.* **2019**, *145*, 04019009. [[CrossRef](#)]
51. Kaczmarek, L.M.; Radosz, I.; Zawisza, J. Numerical Calculations with a Multi-layer Model of Mixed Sand Transport Against Measurements in Wave Motion and Steady Flow. *Rocz. Ochr. Sr.* **2021**, *23*, 629–641. [[CrossRef](#)]
52. Kaczmarek, L.M.; Biegowski, J.; Sobczak, Ł. Modeling of Sediment Transport with a Mobile Mixed-Sand Bed in Wave Motion. *J. Hydraul. Eng.* **2022**, *148*, 04021054. [[CrossRef](#)]
53. Elhakeem, M.; Imran, J. Density Functions for Entrainment and Deposition Rates of Nonuniform Sediment. *Am. Soc. Civ. Eng.* **2012**, *138*, 591–609. [[CrossRef](#)]
54. Sayed, M.; Savage, S.B. Rapid gravity flow of cohesionless granular materials down inclined chutes. *J. Appl. Math. Phys.* **1983**, *34*, 84–100. [[CrossRef](#)]
55. Deigaard, R.A. Note on the three-dimensional shear stress distribution in a surf zone. *Coast. Eng.* **1993**, *20*, 157–171. [[CrossRef](#)]
56. Wong, M.; Parker, G. Reanalysis and correction of bed-load relation of Meyer-Peter and Müller using their own database. *J. Hydraul. Eng.* **2006**, *132*, 1159–1168. [[CrossRef](#)]

Disclaimer/Publisher’s Note: The statements, opinions and data contained in all publications are solely those of the individual author(s) and contributor(s) and not of MDPI and/or the editor(s). MDPI and/or the editor(s) disclaim responsibility for any injury to people or property resulting from any ideas, methods, instructions or products referred to in the content.